Geophys. J. Int. (1992) **109,** 78–95

The resolution of past heat flow in sedimentary basins from non-linear inversion of geochemical data: the smoothest model approach, with synthetic examples

Kerry Gallagher[1,2] and Malcolm Sambridge[3]

[1] *Department of Earth Sciences, Open University, Walton Hall, Milton Keynes* MK7 6AA, *UK*
[2] *Fission Track Research Group, Department of Geological Sciences, University College London, Gower St., London* WC1E 6BT, *UK*
[3] *Institute of Theoretical Geophysics, Department of Earth Sciences, University of Cambridge, Downing St., Cambridge* CB2 3EQ, *UK*

Accepted 1991 October 9. Received 1991 October 9; in original form 1991 March 11

SUMMARY

An inversion technique to reconstruct the heat flow history of a sedimentary basin from downhole geochemical (or thermal indicator) data is presented. The method has been successfully applied to other geophysical inverse problems and attempts to bound a property of the model. This contrasts with the more common approach of merely finding a model which can predict the data, which is less meaningful for underdetermined problems. In this particular application we seek the smoothest model that can predict the observed data to within a given misfit value. This stabilizes the highly non-linear inversion problem and suppresses the generation of complexities in the heat flow history which are unwarranted by the data. Both first and second derivative smoothing constraints are considered, and the differences between the resulting models allows an assessment of the resolution of the heat flow history. Examples are given using synthetic vitrinite reflectance, sterane and hopane isomerization and sterane aromatization data. Our synthetic inversions indicate that for models with accurate thermal parameters, burial history, and thermal indicator predictive models, the heat flow generally cannot be well resolved back past the timing of maximum temperatures, which in many cases is likely to be the present day. The ability of a particular data type to resolve heat flow back in time depends on the effective kinetic parameters which control the rate of reaction as a function of temperature. When realistic uncertainties in the burial history, present-day heat flow and kinetic parameters are considered, false structure may be introduced into the heat flow history and the inversion generated heat flow models can show significant differences from different data types. The algorithm has the benefit of highlighting the degree of non-uniqueness in the problem and provides an efficient way of generating heat flow models which contain the minimum amount of variation necessary to satisfy the observations, thereby reducing the risk of overinterpreting the data.

Key words: heat flow, inversion, smoothest model, thermal indicators.

1 INTRODUCTION

Of the predictions commonly made from geophysical models of sedimentary basin formation, subsidence and surface heat flow histories are potentially among the most useful in constraining the relevant physical mechanisms. For example, the pure shear extension model (McKenzie 1978) predicts an initial period of rapid subsidence and elevated heat flow which subsequently decay exponentially to the steady state values. Simple shear extension models (Wernicke 1985) exhibit similar time dependence; the major difference from the pure shear models is the asymmetry expected across a basin (Buck *et al.* 1988; Voorhoeve & Houseman 1988). Other thermally driven models (e.g. Sleep 1971; Flavey 1974; Middleton 1980; Turcotte & Angevine 1982) predict essentially the same exponential or square root of time dependence to subsidence and heat flow as mentioned above, although the nature of the early part of a

basin's history may differ in detail. A variable subsidence history is expected with foreland basin models (Beaumont 1981; Jordan 1981), dependent on the magnitude and erosion of thrust generated topography adjacent to the evolving basin. As there is no explicit thermal influence involved, the heat flow is predicted to be constant with time. In a related problem, Angevine & Turcotte (1983) considered the temperature history of sediments buried beneath a thrust sheet. In this case the surface heat flow is predicted to vary with time, decreasing at first, then relaxing back up to the steady state value. The compressional model of Lambeck (1983) does not predict a time varying heat flow, while the subsidence rate is expected to increase exponentially with time, at least up to a point where large-scale crustal failure terminates the process.

The ability to constrain and test a model ultimately determines its usefulness. Quantitative analysis of subsidence histories (Sleep 1971; Steckler & Watts 1978) is a tremendously valuable technique for understanding basin evolution, providing a test for particular physical mechanisms (e.g. Middleton 1980; Royden & Keen 1980; Barton & Wood 1984; Bond & Kominz 1984; Hegarty, Weissel & Mutter 1988; Gallagher & Lambeck 1989). The role of the heat flow history in basin modelling had less significance initially but the importance of calculating temperature histories has been recognized as a useful technique in many areas, not least in hydrocarbon exploration (Royden, Sclater & Von Herzen 1980; McKenzie 1981; Middleton 1982; Durand 1984; Beaumont *et al.* 1985; Tissot, Petet & Ungerer 1987; Issler & Beaumont 1989; Deming & Chapman 1989; Burrus & Audebert 1990). Predictive models of subsidence and heat flow histories have been coupled with deterministic formulations of the temperature and time dependence of measurable quantities, or thermal indicators, to provide constraints on thermal histories and tectonic processes in sedimentary basins. These thermal indicators, which need to be sensitive to temperatures of less than about 200 °C, as are generally relevant to sedimentary basins, include vitrinite reflectance (Stach *et al.* 1975; Staplin 1982), individual organic reations (MacKenzie & McKenzie 1983; Sajgó & Lefler 1986), diffusion of argon in feldspar (Harrison & Bé 1983), fission track annealing (Gleadow, Duddy & Lovering 1983; Green *et al.* 1989) and fluid inclusions (Tilley, Nesbitt & Longstaffe 1989).

Generally, most applications have used a forward modelling approach to calculate thermal histories. In this situation, the predicted levels of thermal indicators are compared with the observed value and an assessment is made regarding the suitability of a particular thermal history. As a natural progression from this approach, Lerche, Yarzab & Kendall (1984) used a single parameter search method to estimate the most suitable linear heat flow history from vitrinite reflectance observations. Subsequently, Lerche (1988a, b) has described a refined method where the solution is constrained to be one of a variety of functional forms chosen *a priori*. The parameters controlling the particular function are perturbed in an iterative fashion, from some starting values, so that the misfit between observed and predicted values of thermal indicators is minimized. This methodology has been applied by Lerche and co-workers to a variety of thermal indicator types (Lerche 1990). The fundamental difficulty with the inversion of thermal indicator data is that it does not yield a unique solution. Often, however, a single model is preferred. In the type of approach described above the inherent non-uniqueness of the problem is suppressed by the parametrization of the model and also, if necessary, by numerical damping (during matrix inversion). These processes influence the character of the final solution in a complicated and indirect manner. It can therefore become very difficult to appreciate which features of the resulting heat flow profiles are actually determined by the data and which are merely artefacts of the inversion procedure.

In this paper we examine the problem of estimating a heat flow history from thermal indicator data by applying an inversion procedure which avoids the implicit regularization of earlier techniques and instead seeks the least complex or smoothest model which fits the data to an acceptable level. The basic methodology has recently been applied to inverse problems in electromagnetic sounding (Constable, Parker & Constable 1987) and seismic velocity structure (Sambridge 1990). With this algorithm we are able to gain insight into the degree of non-uniqueness of the problem and also to address, via a series of synthetic inversions, the ability of thermal indicator data to resolve heat flow variations back through time.

2 FORMULATION OF THE FORWARD PROBLEM

2.1 Calculating the thermal history in a sedimentary basin

In detail the thermal state of a sedimentary basin is likely to reflect a variety of processes, including differences in the thermal properties of rock types, the perturbing effects of the hydrodynamic regime, the insulating effect of sedimentation, periods of erosion and climate change and the temperature changes associated with diagenetic reactions. Although 2-D and 3-D thermal models can be formulated to include transient terms and fluid flow (Bethke 1985) some assumptions are commonly made to simplify the calculations. As we use a simple 1-D model to calculate temperature histories in this paper, we shall give a brief overview of the rationale behind these assumptions. However, our conclusions are not affected by the simplicity of our model as we shall be only considering synthetic examples.

It is commonly assumed that the most significant heat transfer occurs in a vertical direction, justified in the absence of rapid horizontal fluid flow (Bethke 1985; De Bredhoeft, Djevanshir & Belitz 1988) or major lateral discontinuities in thermal properties (England, Oxburgh & Richardson 1980). Additional assumptions are that a steady state approximation is appropriate and that heat flow is independent of depth. The validity of this depends on the time- and length-scales involved in the problem. For example, Lucazeau & Le Douaran (1985), Hutchinson (1985) and Kominz & Bond (1986) have shown that predicted surface heat flow can be reduced by a factor of 2 (relative to the deep heat flow) as a result of the deposition of low heat capacity sediments and the more rapid the deposition, the greater the difference. These calculations were made on a lithospheric scale (i.e. over 100 km), but if

we were considering only vertical variations of heat flow within the sedimentary pile (a length scale of 5 km or less), then the assumption of steady state is effectively valid for sedimentation rates of $500\,\mathrm{m\,Myr^{-1}}$ and less (Gallagher 1988). In this case the near-surface heat flow differs from the deep heat flow value, but is effectively constant through the sedimentary pile. Depth-dependent heat flow will occur as a result of vertical fluid flow, and also because of the presence of significant quantities of heat-producing elements (U, Th, K) in the sediments. The former effect is most likely to be significant in geothermal areas, especially in regions where permeability is enhanced by fracturing (Garg & Kassoy 1981) and also at basin margins where near-vertical flow may be enhanced (Smith & Chapman 1983; Andrews-Speed, Oxburgh & Cooper 1984; Majorwicz *et al.* 1985). In most situations, radiogenic heat production within the sediments in a basin is unlikely to contribute more than a few $\mathrm{mW\,m^{-2}}$ to the surface heat flow and can generally be neglected.

In the absence of transient, advection and source terms, heat flow is constant with depth and an appropriate energy equation for the sedimentary column at any time is

$$\frac{d}{dz}\left[K(z)\frac{dT}{dz}\right]=0 \tag{1}$$

where $K(z)$ is the thermal conductivity of the sediments, T is temperature and z is depth. The lower boundary condition at $z=z_b$ is given by the heat flow $Q(t)$ (defined to be positive upwards) into the sedimentary pile from below at time t, and the upper boundary condition at $z=0$ is the surface temperature, $T_s(t)$ at time t. The temperature profile is given by the integral equation

$$T(z,t)=T_s(t)+\int_0^z \frac{1}{K(z')}Q(t)\,dz'. \tag{2}$$

Some forms of $K(z)$ allow an analytical solution to be obtained for the temperature (e.g. McKenzie 1981) but for more complicated reationships, equation (2) may be solved numerically by discretizing the depth variable into a series of N grid points z_n $(n=1,\ldots,N)$ and assuming that the physical properties between successive grid points z_{n-1} and z_n are constant. Equation (2) then becomes

$$T(z_n,t)=T(z_{n-1},t)+\frac{\Delta z_n}{K_n}Q(t) \tag{3a}$$

or

$$T(z_n,t)=T_s+\frac{z_n}{\bar{K}}Q(t) \tag{3b}$$

with $T(0,t)=T_s$, $z_N=z_b$, and where

$$\frac{z_n}{\bar{K}}=\sum_{i=1}^{n}\frac{\Delta z_i}{K_i}$$

and $\Delta z_n=z_n-z_{n-1}$. Clearly, if we specify the burial history for a particular layer, and also the thermal conductivity as a function of depth, we can calculate the temperature history of that layer for any heat flow history, $Q(t)$, from equations (3a) and (3b). The results of thermal history calculations can then be combined with predictive models of thermal indicators to determine the set of observations that would result from a given heat flow model.

2.2 Predicting thermal indicators: vitrinite reflectance and organic reations

As mentioned above, a variety of thermal indicators are used in sedimentary basin studies. An extensive discussion of the methodology is not relevant here and Naeser & McCulloh (1989) provide a recent overview of techniques and applications. In this paper we restrict our study to vitrinite reflectance and three individual organic reactions; sterane and hopane isomerization and sterane aromatization.

The reflectance of the solid organic matter is simply the ratio of reflected light intensity to normal incident light intensity. This property is determined under a reflected light microscope using a photomultiplier and is defined for monochromatic light according to the Fresnel–Beer formula as (Stach *et al.* 1975, p. 263)

$$VR=\frac{(r_s-r_m)^2+r_s^2a_s^2}{(r_s+r_m)^2+r_s^2a_s^2} \tag{4}$$

where r_s and a_s are the appropriate refractive and absorption indices of the sample or standard respectively and r_m is the refractive index of the medium in which the sample is immersed. Liptinite, vitrinite and inertinite are types of kerogen which correspond to different types of organic material in the same sediment and have reflectances which increase in this order. Ideally about 50–100 measurements should be made on a given sample and the results are usually displayed as a frequency histogram. The measurements are cited as a percentage of reflected light, and vitrinite reflectance (VR) values of approximately 0.6 to 1.3 per cent are considered to correspond to the oil generation window and the upper limit for dry gas generation is about 5 per cent (Gretener & Curtis 1982). There are numerous potential problems associated with reflectance measurements and their interpretation (Dow & O'Connor 1982; Castano 1985; Price & Barker 1985). These include contamination of the sample by cave-ins or reworked material, incorrect identification of the type of organic material, impregnation of the sample by liquid hydrocarbons, inhomogeneities and optical anisotropy. Some of these problems are apparent when histograms are drawn and it may then be desirable to define maximum and minimum reflectances. Dembicki (1984) has shown that there can be inconsistency between the measurements of different laboratories of up to 100 per cent as a result of sample preparation and method, although for a given laboratory the results appear to be repeatable. Underwood (1990) quotes a variability of 0.1 per cent reflectance units between three laboratories and states that his own laboratory has an internal consistency to within 0.02 per cent. Therefore, provided that the same laboratory has made all the measurements, a data set from a given base should be internally consistent.

It is accepted that temperature, or thermal energy, is a major factor and reflectance will increase on heating. The other factor which is often assumed to have first-order significance is time, suggesting an Arrhenius type relation. Kinetic, or similarly based, models have been proposed by Lopatin (1971), Waples (1980), Royden *et al.* (1980), Antia (1986), Larter (1989), Wood (1988), and Burnham &

Sweeney (1989). These models assume a time–temperature relationship in which the reaction rate is linear in time and has an exponential or power-law dependence on temperature. Some favour little or no time dependence and interpret the data in terms of the maximum temperature experienced by the sample (Price 1983, 1985; Barker 1983) or the duration of time spent at or near the maximum temperature (Hood, Gutjahr & Heacock 1975; Shiboaka & Bennet 1977).

In order to maximize the potential for recovering heat flow history, we adopt a function with a time dependence. Lopatin (1971) proposed that the reaction rate approximately doubles for a 10 °C rise in temperature over the ranges relevant to oil generation (~50°–150 °C). A variety of integrals forms have been proposed (e.g. Royden *et al.* 1980; Waples 1980; McKenzie 1981; Ritter 1984) and a general maturation function for vitrinite reflectance may be written as

$$Mt = \int_0^t a^{[\alpha T(t') - \beta]}\, dt' \tag{5}$$

where a, α, and β are empirically derived constants. Vitrinite reflectance can generally be calibrated against the maturation function with a relationship of the form

$$\mathrm{Ln}\,(VR) = p + q\,\mathrm{Ln}\,(Mt) \tag{6}$$

(Waples 1980; Middleton 1982; De Bremaecker 1983; Issler 1984; Ritter 1984). To make such correlations, it is necessary to assume the thermal hstory of an area for which data are available. Waples (1980) and Ritter (1984), for example, both incorporate geographically diverse data and in most cases assume that the geothermal gradients have been constant through time. Ritter (1984) proposed that $a = 1.35$ in equation (5). He stated that this value reduces the scatter of a plot of Mt with respect to observed reflectance, compared to the value of 2 favoured by Waples (1980). Issler (1984) also used a value of $a = 2$ and extrapolated the present-day gradient to calibrate reflectance data independently from eastern Canada and Western Australia. His correlations of Mt to observed reflectance (equation 6) differed from that of Waples and he recommended not combining vitrinite reflectance data from different areas as uncertainties in temperature histories are compounded. This is a reasonable proposal especially when taken in conjunction with the comments earlier regarding the inconsistencies between measurements made by different laboratories.

Motivated in part by the somewhat *ad hoc* nature of vitrinite reflectance as a thermal indicator, Mackenzie & McKenzie (1983) examined three individual organic reactions; sterane and hopane isomerization and sterane aromatization. Essentially, the isomerization reactions represent reorganization of the geometry of a hydrogen atom around a particular carbon atom (C-20 for sterane and C-22 for hopane), while the aromatization reactions involves the loss of hydrogen atoms and a methyl group in the conversion from a monoaromatic to a triaromatic steroid hydrocarbon. MacKenzie & McKenzie (1983) and Sajgó & Lefler (1986) give extensive accounts of these reactions. The basic assumptions in this methodology are that only one biologically inherited isomer occurs in the near-surface environment and, as a sediment is buried and experiences higher temperatures, this isomer is progressively converted to another form having different stability and chemical properties. By measuring the relative abundances of the reactant and product isomers (usually by gas chromatography/mass spectrometry), the progress of this conversion can be examined. However, the validity of the assumptions have been questioned recently by Peakman *et al.* (1989) and Abbott *et al.* (1990) who have presented experimental evidence that multiple sources of the isomers exist and that the interpretation of downhole data may be more complex than has been previously considered. However, for the purposes of this paper where we are dealing with synthetic examples, we follow the approach of Mackenzie & McKenzie (1983), outlined briefly below.

The isomer conversions are considered to be temperature dependent according to the Arrhenius law, so that the reaction rate constant (k) is given by

$$k = A \exp\,(-E/RT) \tag{7}$$

where A is the pre-exponential, or frequency, factor, E is the activation energy, R is the gas constant and T is absolute temperature. The pre-exponential factor may also be expressed as a function of temperature,

$$A = \frac{bT}{h} \exp\,(\Delta S/R) \tag{8}$$

where b is Boltzmann's constant, h is Planck's constant and ΔS is the entropy change associated with the reaction. Generally, however, the exponential term involving the absolute temperature is believed to be more significant and so the temperature dependence of A is neglected. The reactions are considered to follow unimolecular first-order kinetics so that, for an irreversible reaction, such as sterane aromatization, the rate of change of the concentration of the reactant, C, is given by

$$\frac{dC}{dt} = -kC \tag{9}$$

and for reversible reactions, such as the two isomerization reactions, the concentrations of the reactant (C_1) and product (C_2) are found by solving

$$\frac{dC_1}{dt} = -k_1 C_1 + k_2 C_2, \tag{10a}$$

$$\frac{dC_2}{dt} = -k_2 C_2 + k_1 C_1, \tag{10b}$$

where k_1 and k_2 are the rates of the forward and reverse reactions, respectively. MacKenzie & McKenzie (1983) give the solutions of equations (9) and (10) in terms of the ratio of the concentrations of the product to the product + reactants. For a constant temperature, the ratio of triaromatic to triaromatic + monoaromatic steroids is given by

$$x = \frac{C_T}{C_M + C_T} = 1 - \exp\,(-k_A t) \tag{11}$$

where k_A is the rate constant of aromatization and x varies from 0 initially to 1 on complete conversion and subscripts have been used to indicate the particular steroid in an obvious fashion. For the isomerization reactions, the ratio of

S to $S+R$ isomers is given by

$$y = \frac{C_S}{C_R + C_S} = \left(\frac{\gamma}{1+\gamma}\right)\{1 - \exp[-(1+\gamma)k_1 t]\} \tag{12}$$

where $\gamma = k_2/k_1$ and $k_1(=k_1)$ is the rate constant of isomerization and it is implicitly assumed that γ is independent of temperature over the range of interest. The value of y ranges from zero to an equilibrium value of about 0.54 for sterane isomerization, and 0.61 for hopane isomerization. When the temperature is a function of time, then equations (11) and (12) are rewritten using equation (7):

$$x = 1 - \exp\left\{-A_A \int_0^t \exp[-E_A/RT(t')]\, dt'\right\} \tag{13}$$

and

$$y = \left(\frac{\gamma}{1+\gamma}\right)\left[\!\left[1 - \exp\left\{-(1+\gamma)A_1 \int_0^t \exp[-E_1/RT(t')]\, dt'\right\}\right]\!\right] \tag{14}$$

where A_A and A_1 are the pre-exponential factors in the two cases. Since the temperature history is related to the heat flow history through equations (3a) and (3b), then the above expressions could also be written directly in terms of heat flow $Q(t)$. This constitutes the solution of the forward problem. From a known heat flow history $Q(t)$ one may use equations (3a, b), (5), (13) and (14) to predict the values of the three types of observables x, y and VR, and make a direct comparison with the data. To simplify the inverse problem somewhat we perform a transformation of data types x, y, and VR to x', y' and Mt where

$$x' = -\ln(1-x), \tag{15}$$

$$y' = -\left(\frac{1}{1+\gamma}\right)\ln\left[1 - \frac{y(1+\gamma)}{\gamma}\right], \tag{16}$$

and Mt is given by (5). The forward modelling equations (13) and (14) may now be replaced with the simpler expressions

$$x' = A_A \int_0^t \exp[-E_A/RT(t')]\, dt', \tag{17}$$

$$y' = A_1 \int_0^t \exp[-E_1/RT(t')]\, dt'. \tag{18}$$

This completes the description of the forward modelling. In the next section we formulate the inverse problem, i.e. that of determining the heat flow history from a set of observations. We then present the inversion algorithm and apply it to a variety of synthetic data sets.

3 FORMULATION OF THE INVERSE PROBLEM

Given a discrete set of observed data, d_i, $(i = 1, \ldots, D)$ we want to find the best set of model parameters, m_j, $(j = 1, \ldots, M)$ to represent the heat flow as a function of time such that the original data can be adequately predicted. The predictive equations (equations 5, 17 and 18) can be written in a general vector form as

$$\mathbf{d} = \mathbf{g}(\mathbf{m}) \tag{19}$$

where $\mathbf{d}$ is the data vector with components d_i (e.g. vitrinite reflectance as a function of depth), $\mathbf{m}$ is the heat flow model vector of length M with components m_j, and $\mathbf{g}$ represents the non-linear relationship between the two [i.e. through equation (3a, b) and (5), (17) or (18)]. In order to estimate the goodness of fit between the observed and predicted values, we define a misfit function, Φ, which is a function of the data residual $(\mathbf{d}_{obs} - \mathbf{d}_{calc})$. It is the aim of the inversion procedure to minimize this misfit function to an acceptable level, given our knowledge of the errors in the data, while only introducing the minimum amount of structure necessary into the model $\mathbf{m}$ [in this case heat flow history, $Q(t)$]. In other words we are seeking to place a lower bound on a particular model property, i.e. the roughness. The standard least-squares method minimizes the L_2 norm, or more simply, the length of the misfit vector, so that

$$\Phi(\mathbf{m}) = \frac{1}{2}[\mathbf{d}_{obs} - \mathbf{g}(\mathbf{m})]^T C_{dd}^{-1}[\mathbf{d}_{obs} - \mathbf{g}(\mathbf{m})] \tag{20}$$

where C_{dd}^{-1} is the inverse data covariance matrix of size $(D \times D)$. If the data errors are uncorrelated then C_{dd}^{-1} is diagonal with elements equal to the inverse variance of each observation, σ_i^{-2}. The first consideration is how to parametrize the model. A discrete inversion approach for the model parameters suggests two alternative forms for the heat flow function. The first is in terms of block functions where the heat flow is constant over discrete time intervals,

$$\begin{aligned} Q(t) &= m_j \quad t_j \le t < t_{j-1}, \quad j = 1, \ldots, M, \\ &\quad 0, \quad \text{otherwise} \end{aligned} \tag{21a}$$

where t_N is the present day, and t_0 is the beginning of deposition. The second parametrization is a polynomial in time,

$$Q(t) = m_1 + m_2 t + \cdots + m_M t^{M-1}. \tag{21b}$$

The linear function used by Lerche *et al.* (1984) is a special case of the second form and Lerche (1988a, b, 1990) has suggested other functions to represent Q over time. In this work we wish to use a parametrization which imposes the least constraint possible on the form of the final model and allows it to be as flexible as required. In this way we encourage the heat flow model to be underdetermined, which more closely represents the real situation. All influence on the character of the model which is not due to the data can then be controlled directly by some explicit smoothness constraint and is not forced upon us by the parametrization. The block function representation given by (21a) is most suitable for this purpose. In all cases considered here the blocks had a width of ≤ 2 Myr which gives reasonable confidence that variations in the heat flow of time-scales greater than this were sufficiently overparametrized. Gallagher (1988) examined the inversion problem using a form of the Marquardt method (Fletcher 1971) and found that as a result of the non-linear nature of the model formulation, it was necessary to impose severe damping on the movement of the parameters in model space to obtain stability and reach feasible solutions (e.g. non-negative heat flow, or values less than 500 mW m^{-2}). Consequently, it was observed that, although the data could be adequately predicted, the solutions depended on the initial guess for the solution and the number of iterations, indiating that the

problem is highly non-linear. In order to stabilize the procedure and impose our condition of seeing the simplest model we need to regularize the problem. To do this we follow Constable *et al.* (1987) and Sambridge (1990), by introducing a roughness function, $\psi(\mathbf{m})$ which is minimized jointly with the data misfit function Φ, i.e. we seek the minimum of $U(\mathbf{m})$, where

$$U(\mathbf{m}) = \mu\psi(\mathbf{m}) + \Phi(\mathbf{m}). \tag{22}$$

The scalar μ controls the relative importance of smoothing the model and fitting the data. A large value of μ leads to a greater amount of smoothing and as μ is reduced, the model can become rougher if necessary in order to decrease the data misfit. As outlined in Constable *et al.* (1987), we choose a large value of μ initially and attempt to keep it as large as possible while obtained a satisfactory fit to the data (as determined from the observed or assumed errors). Therefore, we are trying to find the smoothest (least rough) heat flow model that can explain the observed data. The inference is that any structure produced in the model is the minimum required to satisfy the data, but more complexity is not warranted by the data. Therefore, although the final model may not in fact be the true solution, the data alone cannot allow us to distinguish betwen the two. This approach not only has the advantage of stabilizing the inversion procedure but allows us to address the ability to resolve past heat flow from thermal indicator data.

We use two discrete roughness functions which are similar in form to the finite difference first and second derivatives of the heat flow with a constant time interval, i.e.

$$R_1 = \sum_{j=2}^{M} (m_j - m_{j-1})^2 \tag{23a}$$

and

$$R_2 = \sum_{j=2}^{M-1} (m_{j+1} - 2m_j + m_{j-1})^2 \tag{23b}$$

so in vector form, we can write

$$\psi(\mathbf{m}) = \mathbf{m}^{\mathrm{T}}\boldsymbol{D}^{\mathrm{T}}\boldsymbol{D}\mathbf{m} \tag{24}$$

and the elements of the matrix $\boldsymbol{D}$ are given by the coefficients of the m_j in (23a, b) (see Constable *et al.* 1987 for more details). The procedure to minimize the objective function (22) follows to some extent that described by Sambridge (1990) where we adopt an iterative approach, using a locally linearized form of the problem and solve for model perturbations $\delta\mathbf{m}$. The algorithm is derived in Sambridge (1990) and the reader is referred to that paper for the details. For the kth iteration, the model update is given by

$$\delta\mathbf{m}_{k+1} = (\mu\boldsymbol{D}^{\mathrm{T}}\boldsymbol{D} + \boldsymbol{G}^{\mathrm{T}}\boldsymbol{C}_{\mathrm{dd}}^{-1}\boldsymbol{G})^{-1} \times \{\boldsymbol{G}^{\mathrm{T}}\boldsymbol{C}_{\mathrm{dd}}^{-1}[\mathbf{d} - \mathbf{g}(\mathbf{m}_k)] - \mu\boldsymbol{D}^{\mathrm{T}}\boldsymbol{D}\mathbf{m}_k\} \tag{25}$$

where $\boldsymbol{G}$ is the matrix of partial derivatives of $\mathbf{d}$ with respect to $\mathbf{m}$, so that $G_{ij} = \partial d_i/\partial m_j$. Because of the non-linearity of the problem these deriatives also depend on the model parameters m_j and are recalculated after each model update. These derivatives may be determined for the thermal indicator functions considered in this paper using the formulae in the Appendix. After evaluating (24) the new model is given by

$$\mathbf{m}_{k+1} = \mathbf{m}_k + \alpha\delta\mathbf{m}_{k+1}. \tag{26}$$

Here, the vector $\delta\mathbf{m}_{k+1}$ is the direction in model space in which the model $\mathbf{m}_k$ is perturbed, while the scalar α controls how far we move in that direction. In most cases, α is equal to 1 and we use the full model step. However, if the model step is such that it causes a new model parameter to become unfeasible (i.e. negative), we choose α so that the update to this parameter results in the new value being equal to 0, and all other parameter values ≥ 0. The solution of equation (24) involves the inversion of an $M \times M$ matrix where M is 60 for our examples and this presents no great difficulties computationally. As a practical consideration, we found it useful to be able to constrain the heat flow value at the present day (model parameter m_M) to a given value. This is a reasonable approach given that there is usually some information on the present-day thermal state of a exploration well, notwithstanding the problems associated with downhole temperature measurements (Hermanrud, Cao & Lerche 1990). We choose to use the Lagrange multiplier approach (e.g. Menke 1984) and fix the Mth model parameter to a prescribed value (i.e. calculated present-day heat flow). A more flexible approach would perhaps be to use the method proposed by Tarantola & Valette (1982) where an *a priori* probability distribution is determined for each model parameter. Thus the most recent heat flow value could be prescribed a relatively small uncertainty, reflecting the information we may have on that model parameter, while the other model parameters would have large uncertainties.

In implementing the algorithm given by equation (25), we need to specify a value for μ. As a consequence of the relative ease of the forward modelling and calculation of partial derivatives, we can use the 1-D line search scheme of Constable *et al.* (1987). Therefore, we specify a large value of μ initially and sweep through progressively lower values until we find a minimum with line search, in which case we use this solution in the next iteration, or the inversion converges to an acceptable solution given by a specified misfit level, Φ_*, determined by the uncertainties in the data. In our synthetic inversions this misfit level is chosen to be equal to D, the number of data and in practice we search for the largest value of μ that predicts $\Phi_* = D$. This is the expectation value for a data set whose errors are independent and follow a Gaussian distribution with zero mean.

4 RESULTS

4.1 Modelling procedure

To illustrate the application of the inversion technique to heat flow history modelling, we generated a series of synthetic data sets. Unless otherwise stated, these were calculated as follows: a subsidence history was specified for 120 Myr, consistent with the model of McKenzie (1978) with a stretching factor (β) of 1.4 although the period of initial subsidence occurred over 20 Myr at a constant rate. Sediment was assumed to have infilled the basin at all times with porosity reduction occurring by compaction and Gallagher & Lambeck (1989) detail the necessary

Table 1. Parameters used for modelling. The vitrinite reflectance parameters are from Royden *et al.* (1980) and De Bremaecker (1983) and the parameters for the three organic reactions are from MacKenzie & McKenzie (1983).

Model	function	parameter values
Porosity (ϕ)	$\phi(z) = \phi_0 e^{-cz}$	$\phi_0 = 65\%$ $c = 1.2\times10^{-3}$ m^{-1}
Thermal conductivity (K)	$K = 0.5*(K_g + K_m)$ $K_g = K_s^{1-\phi} K_f^{\phi}$ $K_m = K_s \cdot \frac{(2r+1) - 2\phi(r-1)}{(2r+1)+\phi(r-1)}$ $r = K_s / K_f$	$K_s = 2.5$ Wm^{-1}K^{-1} $K_f = 0.61$Wm^{-1}K^{-1}
Density (ρ)	$\rho = (1-\phi)\rho_s + \phi\rho_f$	$\rho_s = 2900$ kgm^{-3} $\rho_f = 1000$ kgm^{-3}
Vitrinite reflectance (VR)	see eqs. 5,6	$a = 2, \alpha = 0.1, \beta = 0$ $p = 0.173, q = -2.242$
Sterane aromatisation (SI)	see eq. 13	$E_A = 200$ kJmol^{-1} $A_A = 5.68\times10^{27}$/m.y.
Sterane isomerisation (SI)	see eq. 14	$E_I = 91$ kJmol^{-1} $A_I = 1.89\times10^{11}$/m.y. $\gamma = 1.174$
Hopane isomerisation (HI)	see eq. 14	$E_I = 91$ kJmol^{-1} $A_I = 5.05\times10^{11}$/m.y. $\gamma = 1.564$

formulations for this problem. The thermal conductivity in the sediment was calculated as the average of the Maxwell and geometric means for a two-phase medium, a model appropriate for sediments in the Eromanga Basin, Australia (Gallagher 1987) and the thermal conductivity was considered to be independent of temperature. Internal heat production was not included. The relevant values for parameters used in these calculations are given in Table 1. It should be stated at this point that the results discussed subsequently are independent of the values chosen for these parameters as identical values were used in the forward and inverse model runs. After specifying a particular heat flow history, the thermal history of any stratigraphic horizon was calculated for 20 horizons at 6 Myr intervals, commencing at 120 Ma and maturation integrals for these 20 horizons were calculated for vitrinite reflectance using the maturation function proposed by Royden *et al.* (1980) and De Bremaecker (1983) (equations 5; model VR) and also for sterane aromatization (equation 17; model SA) and both sterane and hopane isomerization (equation 18; models SI and HI). The constants used in these integrals are given in Table 1. In using these models we are not implying that these are necessarily the correct formulations or parameters to use for predicting vitrinite reflectance or the organic reactions, rather they provide a convenient framework in which to test the inversion procedure. Subsequently, we shall investigate the consequences of using inappropriate predictive functions for reconstructing heat flow histories, such as different maturation integrals for vitrinite reflectance and differing kinetic parameters for the organic reactions. Fig. 1(a) shows the burial history for 20 horizons and Fig. 1(b) shows the porosity–depth and thermal conductivity–depth functions. The thermal histories for the 20 horizons with a constant heat flow of 50 mW m^{-2} are shown in Fig. 1(c) and the predicted thermal indicator levels are given in Fig. 1(d).

The inverse modelling procedure was as follows: a heat flow history was specified and a synthetic data set generated. This data was then used as input to test the inversion algorithm with the heat flow parametrized as a series of block functions ($M = 60$). The initial model guess was set equal to the present-day heat heat flow (as might be calculated from downhole temperature measurements and assumptions or observations regarding the thermal conductivities of the lithologies) and the final parameter was constrained to that value. All values used in the reconstruction of the burial history were exactly those used in the forward model, so no uncertainty is introduced through an incorrect burial history or thermal parameters. The *a priori* errors were specified as 0.004 units for all data types prior to the transformations performed to simplify the forward modelling (equations 6, 17, 18). The errors on the transformed values were calculated by taking average of the spread of the raw values after the same transformation. The error value of 0.004 is intentionally an order of magnitude less than would commonly be adopted for the aromatization and isomerization measurements (MacKenzie & McKenzie 1983) and vitrinite reflectance measurements (Underwood 1990). Therefore, we are being overoptimistic with the quality of both the thermal indicator data and our knowledge of the burial history and thermal conductivities. Consequently, when the inversion algorithm converges to a solution (i.e. predicts the data to within these errors), the heat flow model can be regarded as providing a near-perfect fit to perfect data and we can directly address the ability of such data to resolve past heat flow. If larger errors are considered it then becomes more important to add in the noise to the synthetic data to avoid significantly biasing the solution (Constable 1991). At this stage, we need to point out that because the progress of the individual organic reactions tends to limiting values, we only use the data down to the most shallow depth where the relevant equilibrium value occurs. This is because the thermal history of all points below this depth will necessarily have been hotter [which follows from using equation (3a)], but we cannot constrain how much hotter.

4.2 Resolving heat flow variations with a perfect forward model

We shall initially consider a few different forms of heat flow history, while always using the same burial history. In general, the heat flow histories used are not considered to represent any particular tectonic mechanism; rather we wish to test the ability of our algorithm to resolve heat flow variations and examine how well we can reconstruct the original form. However, the first model we consider is a reasonable representation of the heat flow expected from an extensional basin with an extension factor (β) of 1.4. In this model, an initially high heat flow decays back to the initial steady state value (McKenzie 1978; Jarvis & McKenzie 1980; Cochran 1983). The inversion results are summarized in Fig. 2. The solutions obtained by minimizing the first derivative of the heat flow history [i.e. using the roughness function in equation (23a)] are shown in Fig. 2(a). In this case the inversion algorithm keeps the heat flow flat unless the data demands otherwise, and one can see that although there is a hint of an increase in heat flow back to about

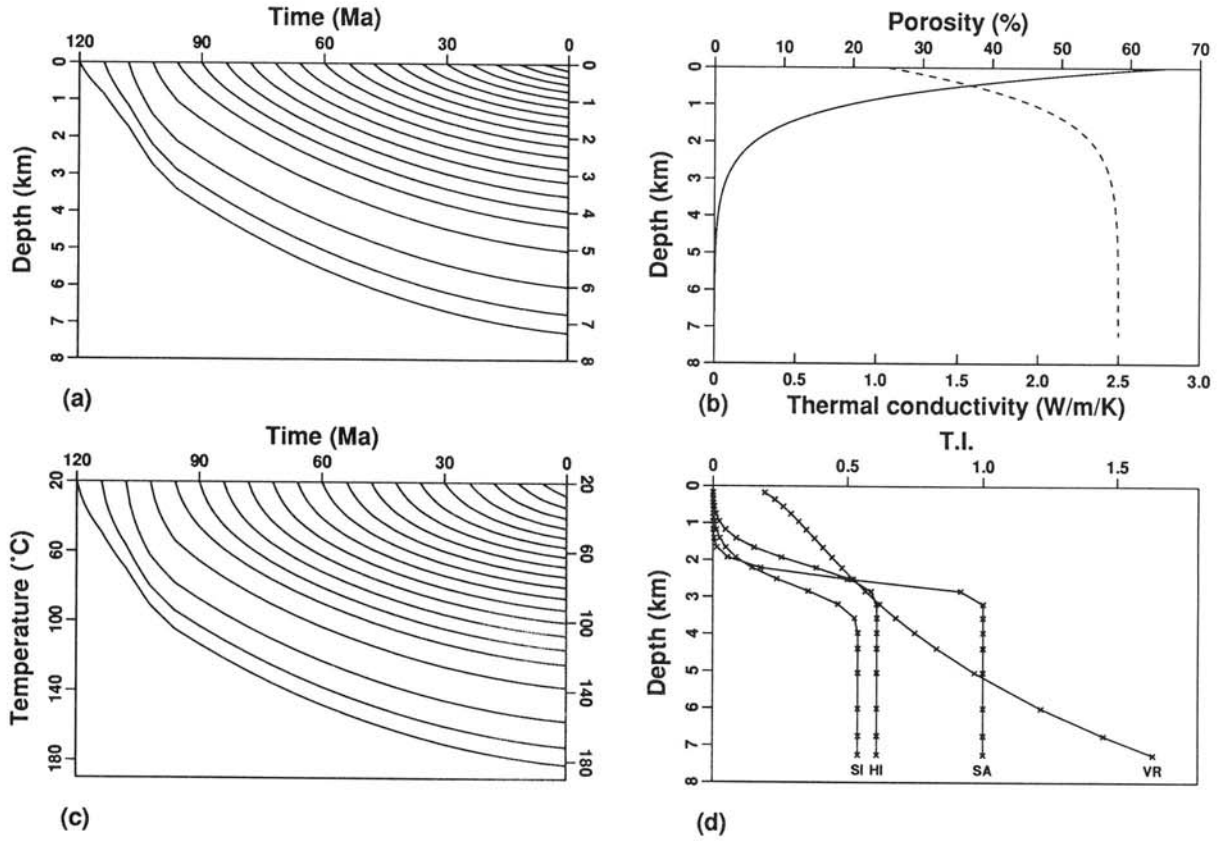

Figure 1. (a) Burial history calculated for 20 horizons at intervals of 6 Myr with the McKenzie model ($\beta = 1.4$) and continuous sediment infill. The initial subsidence is assumed to have occurred over 20 Myr, rather than instantaneously. (b) Porosity (solid line) and thermal conductivity (dashed line) depth functions used for the calculations. (c) Thermal histories for the 20 layers calculated with $Q = 50\,\text{mW m}^{-2}$ and $T_s = 20\,°\text{C}$. (d) Predicted levels of thermal indicators (T.I.) as a function of depth. VR = vitrinite reflectance, SI = sterane isomerization, SA = sterane oramatization, HI = hopane isomerization.

25–30 Ma, the data are generally consistent with a relatively constant value. The solutions obtained by minimizing the second derivative [i.e. using the roughness function in equation (23b) are shown in Fig. 2(b). In this case the algorithm tries to keep the gradient of the heat flow constant and is able to maintain the increasing heat flow back through time, although the gradient flattens off slightly at about 60 Ma. In this particular model we are dealing with small variations in heat flow as result of the low value of β and it is perhaps not unexpected that we cannot resolve the early heat flow high of the original model shown as the dotted line in Figs 2(a) and (b). However, similar results are obtained when larger extension factors are used, suggesting that it is unlikely that rift-related heat flow variations could be resolved from thermal indicator data within a basin of this age. This is essentially because the sediments are currently at their maximum temperatures and the power or exponential dependence of the thermal indicator integrals on temperature reduces the signficance of the earlier, lower temperature part of the sediments' thermal history. This conclusion is in broad agreement with the results of McKenzie (1981) who showed that rocks in rift basins will be at their maximum temperatures, unless they were at depths of more than about 4 km when the heat flow maximum occurs.

We stress that an interpretation of such data in terms of rift induced heat flow variations is not ruled out (indeed, in this case, it is the true answer). However, we have shown that the data are also consistent with a relatively invariant heat flow history and therefore additional evidence would need to be obtained before invoking a more complex model. It is interesting to note at this stage that where the two different smoothing models most closely agree with each other, they agree with the true answer. This is more clearly seen in subsequent models and suggests that it may be useful to some extent to use both types of smoothing in order to address the ability to resolve the heat flow back through time.

The next two heat flow models we consider are smooth single wavelength sine functions with a mean value of $50\,\text{mW m}^{-2}$ and a variation about this mean of $\pm$ $20\,\text{mW m}^{-2}$ (see Figs 3a and 4a). The models both have wavelengths of 120 Myr, one with decreasing heat flow up to the present day and the other with increasing heat flow. The results for the former case are shown in Fig. 3 and clearly the statement above regarding the lack of resolution of heat flow past the time of maximum temperature (<30 Ma) is supported. The shallowest samples reach their maximum temperatures at the present and it is clearly the timing of the deeper samples' maximum temperature that is important.

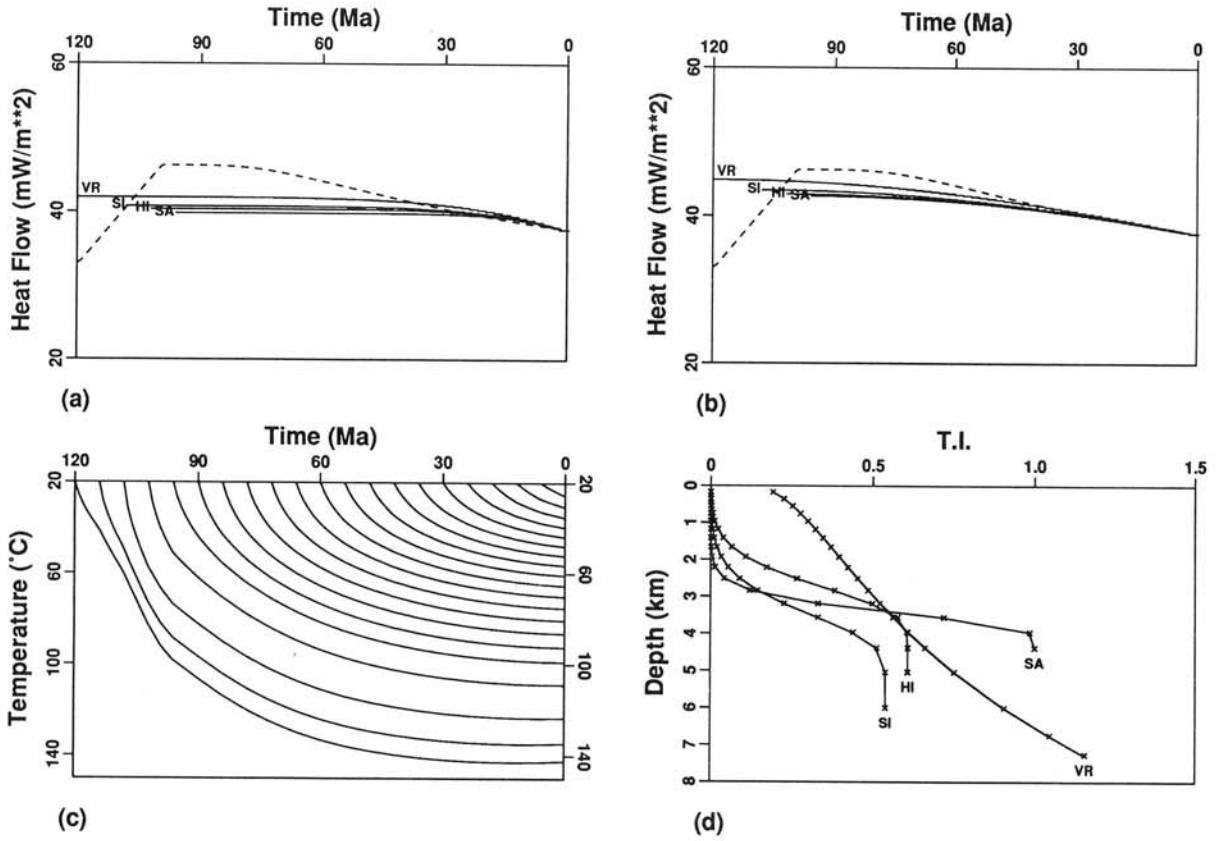

Figure 2. (a) True heat flow (dashed) and inversion results for the four thermal indicator types with first derivative smoothing. (b) As in (a) but with second derivative smoothing. (c) Thermal histories for the 20 layers when the heat flow increases linearly for the first 20 Myr then decays according to the McKenzie (1978) model with $\beta = 1.4$. (d) Predicted levels of the thermal indicators as a function of depth. The x mark the input (observed) data and the solid lines join up the predicted values. Note that the input data for the three organic reactions is truncated at the depth of the first value to reach the equilibrium level.

Also, the deviation between the first and second derivative results again occurs at about the same time as the deeper samples' maximum temperature. The situation in the latter case where the heat flow increases to the present day (Fig. 4) is slightly more complicated in that temperature values near the actual maximum (occurring at the present day) were experienced by the deeper samples at around the time that the heat flow was at its maximum value (~90 Ma). This illustrates the influence of the type of thermal indicator on the resolution of the heat flow history. The vitrinite reflectance model can resolve the heat flow reasonably well back to about 90 Ma, whereas the sterane and hopane isomerization models can only go back to about 60 Ma at best and the sterane isomerization model can only adequately resolve the heat flow back to about 20 Ma. This observation is partly attributable to the differing effective kinetic parameters [E and A in equation (7)] controlling the reaction rate for each function. The results with second derivative smoothing show that, of the organic reactions, the lowest activation energy and frequency factor reaction (SI) potentially has the best resolution back in time, while the reaction with the largest values (SA) has the worst. The first derivative smoothing results show a similar trend but the heat flow models actually differ less. Higher activation energies and pre-exponential factors result in rapid reaction rates but the reaction effectively commences only after a critical temperature has been reached, whereas lower values of these values tend to distribute the reaction progress over a wider temperature range and the reaction effectively starts at lower temperatures. The rate of increase of the rate constant, k, for the organic reactions decreases with increasing temperature, but is greater than 2 for every 10 °C increase over values less than 120 °C, by which time equilibrium is reached. The doubling of reaction rate for 10 °C increase in temperature for the vitrinite model leads to a temperature-dependent activation energy, but an effective value for 50 °C is ~62 kJ mol^{-1}, and this increases by about 5 kJ mol^{-1} for every 10 °C increase in temperature up to 200 °C. Therefore the organic reactions tend to show greater non-linearity to temperature than the vitrinite reflectance.

The resolution is also influenced by the fact that the three organic reactions all tend to a finite value. As explained earlier, this means that thermal history can only be resolved back as far as the age of the shallowest data point at this equilibrium value, at least in a well where only vertical movement of sediment has occurred (i.e. no repetition of strata or overthrusting). In contrast, the vitrinite model potentially allows the full thermal history to be reconstructed because the predicted values keep increasing with higher temperatures. Another probably influence is that the present-day maximum temperature of the three deepest samples is less than 25 °C greater than the maximum

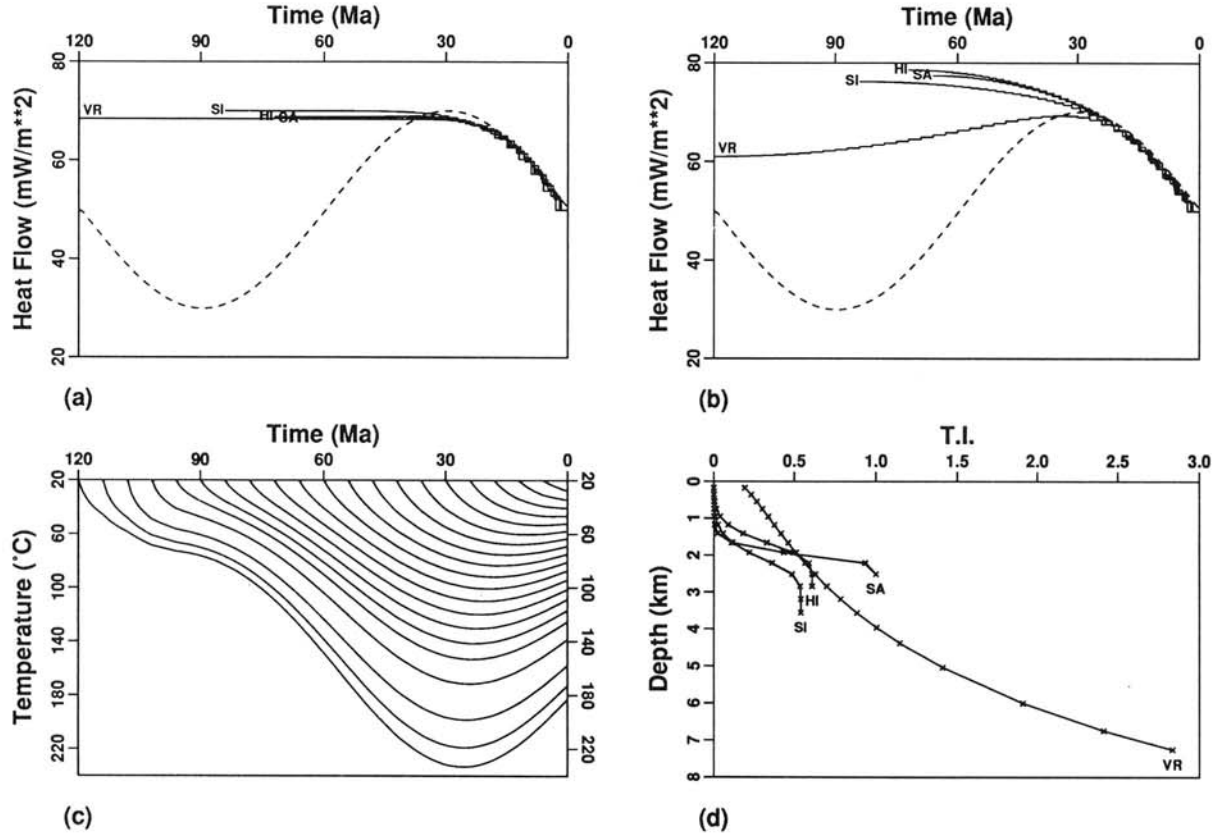

Figure 3. Results for a sinusoidal variation in heat flow, $Q = 50 + 20 \sin [\pi(60 - t)/60]$ mW m^{-2}. Other details as for Fig. 2.

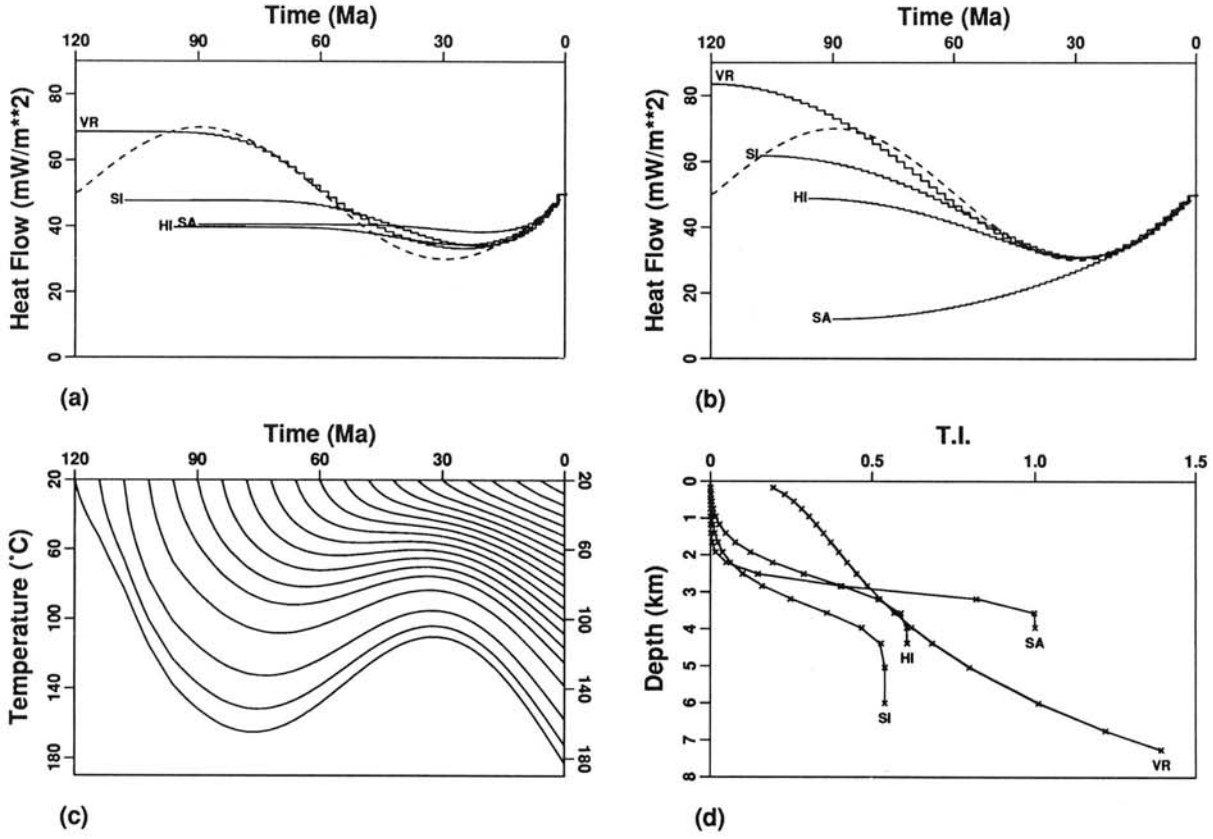

Figure 4. Results for a sinusoidal variation in heat flow, $Q = 50 - 20 \sin [\pi(60 - t)/60]$ mW m^{-2}. Other details as for Fig. 2.

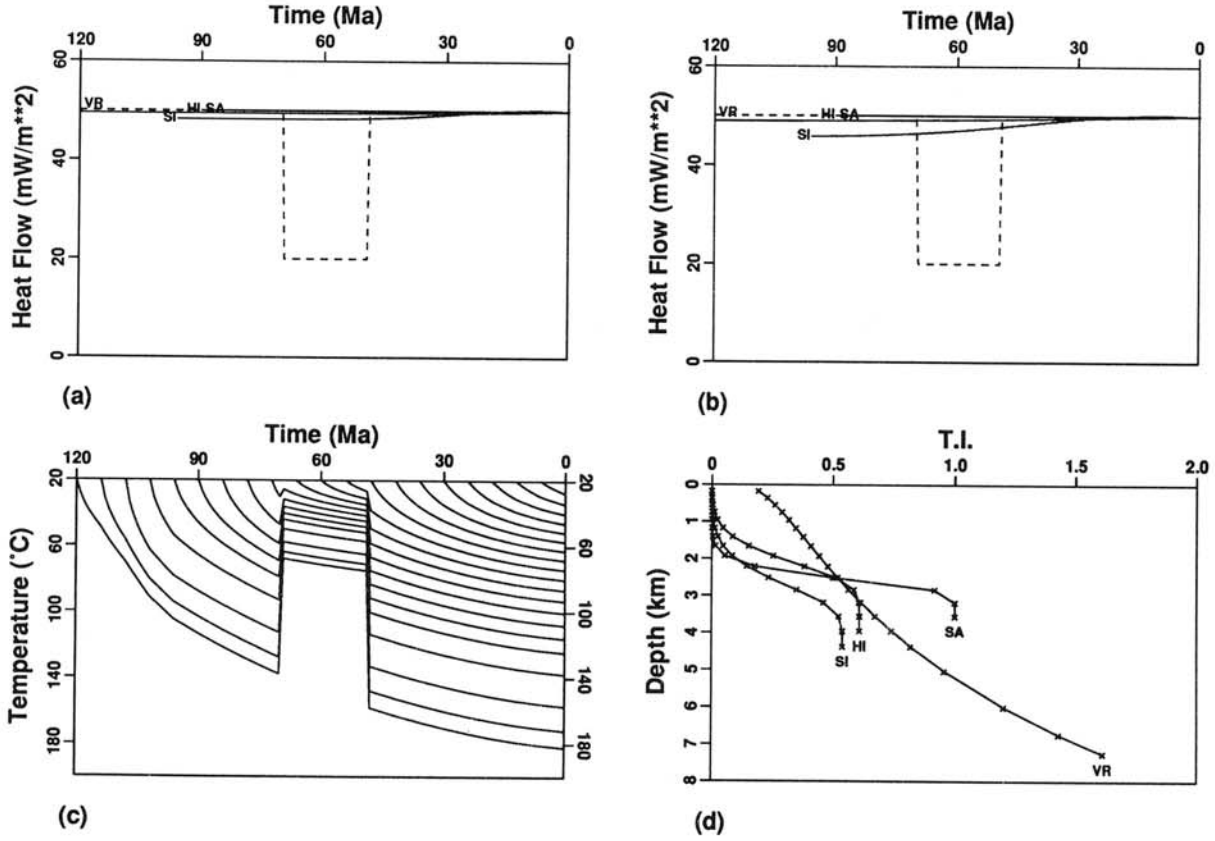

Figure 5. Results for $Q = 50\,\text{mW m}^{-2}$ except for $t = 50$–70 Ma when $Q = 20\,\text{mW m}^{-2}$. Other details as for Fig. 2.

experienced at ~85 Ma. All the more shallow samples have differences of at least 30 °C between the present-day temperature and any previous localized maximum. This tends to support the proposition that a model based on the amount of time spent near to the maximum temperature is adequate to predict maturation levels (Hood *et al.* 1975; Shiboaka & Bennett 1977; Beaumont *et al.* 1985). If heat flow models with two wavelengths in the 120 Myr time span are considered, we again can only really resolve the heat flow back to about the timing of maximum temperature experienced by the deeper layers, again supporting that conclusion.

As a final pair of examples in this section we consider a situation where a heat flow pulse occurs over a limited time, while burial is continuous. In these cases we have a constant heat flow of $50\,\text{mW m}^{-2}$ and a perturbation of $\pm 30\,\text{mW m}^{-2}$ occurs between 70 and 50 Ma. We can see that the data tells us very little about the case where the heat flow decreased (Fig. 5) and we cannot use the agreement between the first and second derivative smoothing solutions as a guide to the validity of our answer, as both give a near constant heat flow value. In the case where the heat flow increases (Fig. 6), the data allow us to resolve the fact that heat flow has increased in the past. The departure between the first and second derivative cases occurs at about the time of maximum temperature which, in this case, coincides approximately with the time of maximum heat flow. However, we have little confidence regarding the true magnitude of the maximum or the heat flow regime prior to this time. In these last two cases, the algorithm has performed as expected, leading to smooth solutions which are lower bounds on the roughness of the true model. However, the smooth models are not necessarily good representations of the true answer. In Fig. 6 for example, the data are only sensitive to the later decreasing half of the pulse and so the increasing half does not appear in the smooth models. This highlights the care that must be taken in interpreting the results of the smooth inversion. They provide the user with a bound on the roughness of the heat flow model and must not be treated too literally as direct estimates of the true model, else one may be misled in cases where the true heat flow functions have discontinuities. These two examples, however, do demonstrate the lack of resolution of past heat flow and the fact that the solutions are non-unique. We have examined the resolution of a similar heat flow pulse occurring closer to the present day (occurring between 10 and 30 Ma). These results are not shown here, but we found that when the heat flow increases, the results are similar to those shown in Fig. 6, i.e. we cannot resolve structure past the timing of the maximum temperature. When the heat flow decreases, the broad structure of the inversion models reflects the true answer in that the heat flow initially decreases when increases back in time. However, the overall wavelength of the heat flow variation is broader than the true answer, reflecting the influence of our smoothing constraints and the lack of resolving power in the data.

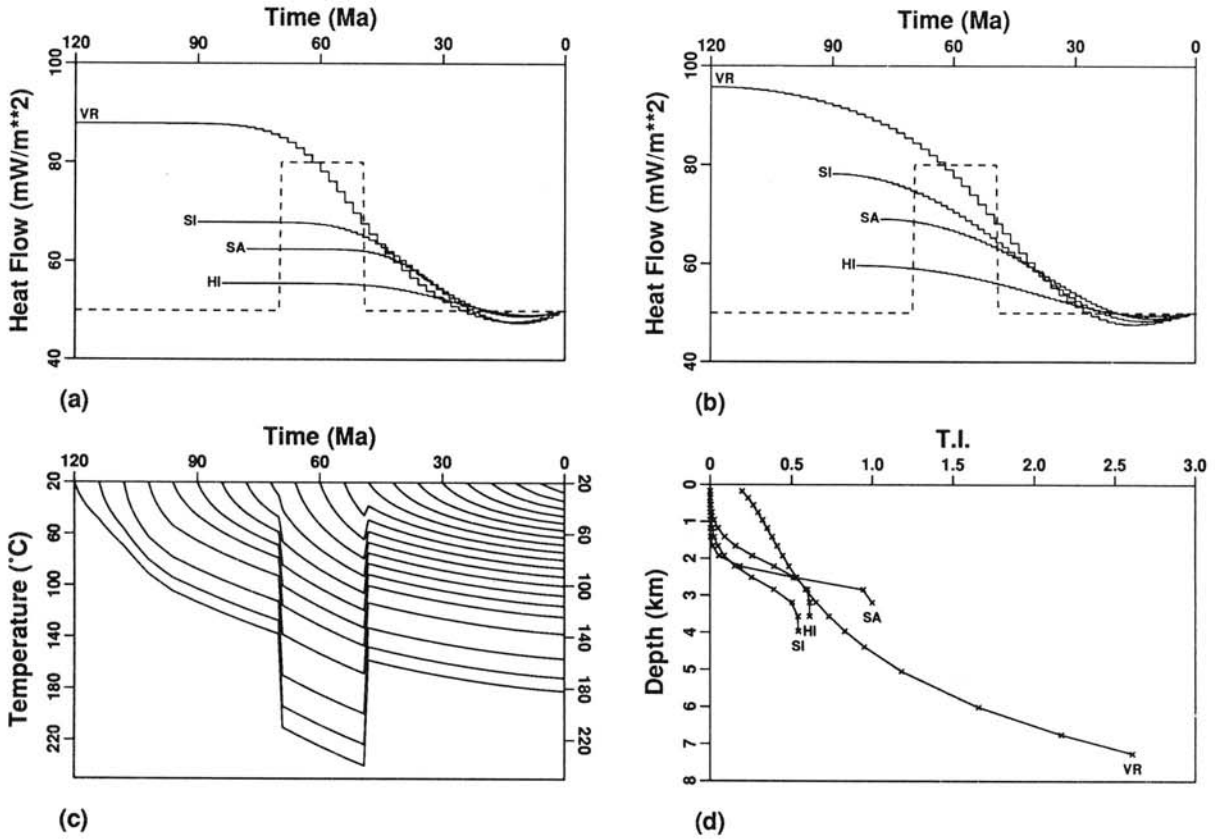

Figure 6. Results for $Q = 50\,\mathrm{mW\,m^{-2}}$ except for $t = 50$–70 Ma when $Q = 80\,\mathrm{mW\,m^{-2}}$. Other details as for Fig. 2.

4.3 The influence of erroneous assumptions in the forward modelling

In this section we consider a few examples where our forward modelling is not as precise as we might wish. Specifically, we look at situations where the present-day heat flow is constrained to an incorrect value, where a period of erosion occurs but is modelled as a period of non-deposition and where the parameters values in the maturation functions differ between the forward modelling and inversion.

4.3.1 Errors in the bottom hole temperature

Firstly, we examine the case where present-day heat flow is incorrectly estimated, as may occur when downhole temperature measurements are inaccurate. In the absence of a specifically designed temperature survey, it is common practice to use temperatures measured during downhole logging as constraints in thermal history modelling for exploration purposes. In these situations it is well known that the observed temperatures need to be corrected to account for cooling due to the circulation of drilling fluid and, to this end, a variety of methods are in use (see Hermanrud *et al.* 1990). Under the assumption of steady state conditions, heat flow may be easily estimated from corrected downhole temperature values, provided measurements or assumptions are made regarding the thermal conductivity of the rock types encountered in the drill hole and also a value is chosen for the mean near-surface temperature. This method is known as the Bullard or thermal resistance method and has been used in regional studies to estimate heat flow from the bottom hole temperature in wells (Chapman *et al.* 1984; Andrews-Speed *et al.* 1984; Majorwicz *et al.* 1985). As an example, we look at the case where only the bottom hole temperature is used to calculate the present-day heat flow, and the value of this temperature is 10 °C less than the correct value. This represents an error of about 5 per cent and is within commonly assumed uncertainties (Andrews-Speed *et al.* 1984; Hermanrud *et al.* 1990). The calculated present-day heat flow is about $3\,\mathrm{mW\,m^{-2}}$ less than the true value. The results are given in Fig. 7 and show what one might expect, that the heat flow functions initially increase relatively rapidly by about 25–30 Ma to a value slightly higher than the true heat flow to compensate for the low present-day heat flow. The first derivative models then flatten off back in time while the second derivative models diverge. Over the time where the final heat flow models are reasonably consistent, they are within 5 per cent of the true value and the maximum temperatures experienced by the deeper layers are close to their true maximum temperatures, although they occur at earlier times. Broadly similar results are obtained for the case where the bottom hole temperature is overestimated, except the heat flow models compensate by decreasing back in time before they flatten off or diverge.

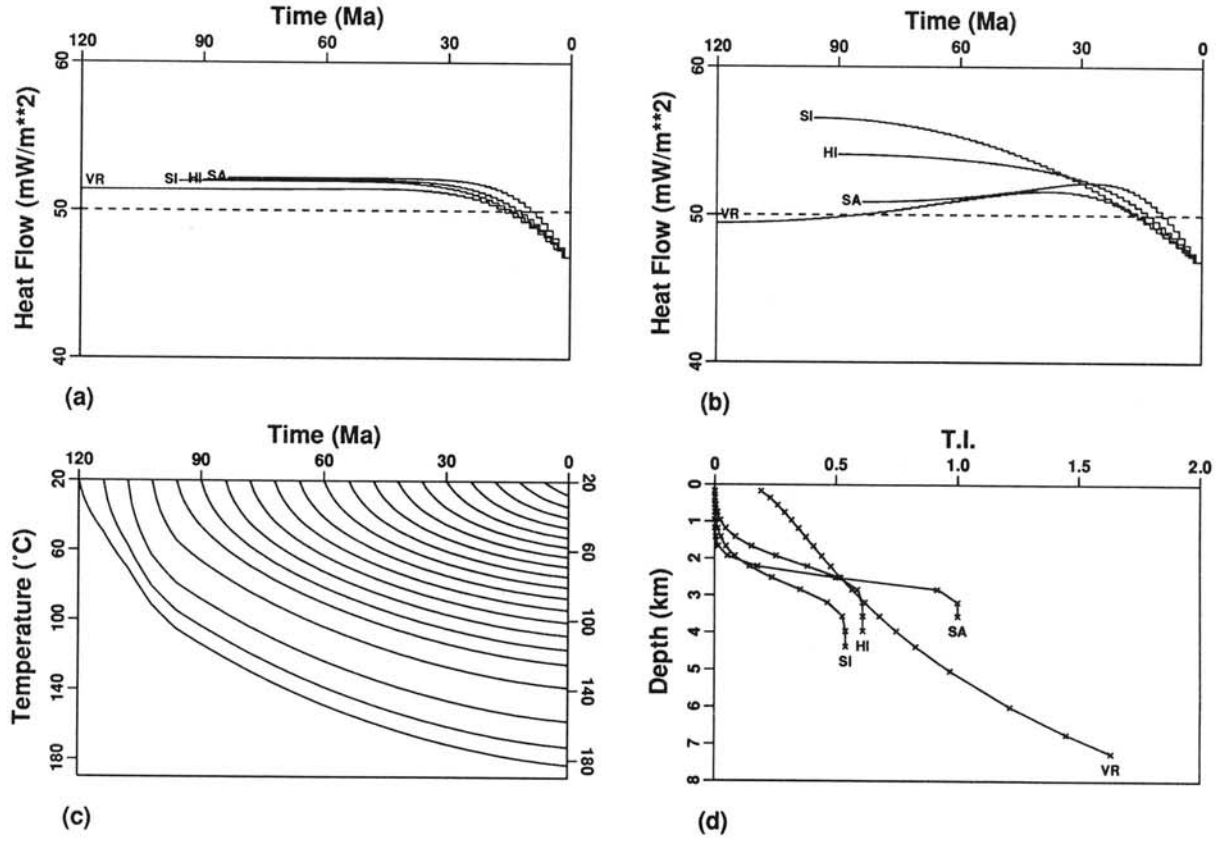

Figure 7. Results when the bottom hole temperature is 10 °C too low. The input data were calculated with $Q = 50\,\text{mW m}^{-2}$ and for the inversion the present-day heat flow was constrained to be $47\,\text{mW m}^{-2}$. Other details as for Fig. 2.

4.3.2 Errors in the burial history due to erosion

Next we consider the case where a period of erosion occurred, removing part of the sedimentary section. In this case, we use a different burial history to the previous models such that our well encounters 3000 m of sediment where the bottom hole temperature in the well is 120 °C, equivalent to a heat flow of $\sim 65\,\text{mW m}^{-2}$. The age at the top of the well is 0 Ma, with an age increase of 10 Myr for every 300 m of sediment. An unconformity occurs at 1500 m and spans 50–80 Ma so that the age at the base of the well is 130 Ma. The original thermal indicator data was calculated with deposition of 2000 m of sediment between 80 and 65 Ma and then this was removed linearly between 65 and 50 Ma. However, the resulting unconformity was modelled as a period of non-deposition in the burial history used in the inversion. In this and the following example, the errors were set to 0.01, to allow a greater uncertainty in predicting the data. These values are still lower than would be routinely used. The results are shown in Fig. 8 and clearly neglecting the period of deposition/erosion has a significant effect on introducing false structure into the solution. If we were to use the criterion that we accept as reasonable the heat flow up to the point where the first and second derivative solutions diverge, we would not want to go back much further than 10 Ma. In this run, the algorithm did not actually converge to the desired level of misfit and the iterative process was terminated when no further reduction of the misfit function occured. It is not surprising we had difficulty, considering of the magnitudes of discontinuities in the observed data across the unconformity. In order to achieve required misfit level for convergence, the error on each datum would need to be increased by a factor of about 2 for models VR and SI, a factor of 4 for HI and 8 for SL. Of course, if less erosion had occurred, the discontinuities would be reduced but it is obviously advisable to closely sample either side of suspected unconformable surfaces to ensure that discontinuities in thermal indicator data and significant loss of section could potentially be resolved. By modelling the unconformity as a period of non-deposition, we have really considered the worst case by not allowing for any removal of section. Lerche (1988b) has also examined the problem of estimating the thickness of missing section and showed that it is straightforward to try and optimize the estimate with a search method. In related studies to the problem of unconformities, Katz, Pheifer & Schunk (1988) and Majorwicz *et al.* (1990) concluded that, in practice, noise in vitrinite reflectance data would often reduce the accuracy of such estimates considerably and Middleton (1982) has shown that it is difficult to constrain the timing and duration of periods of erosion.

4.3.3 Errors in the maturation functions

The maturation functions used for the example calculations in the preceding sections are not considered unique. As mentioned in section 2.2, a variety of different functions have been proposed to predict vitrinite reflectance. Also

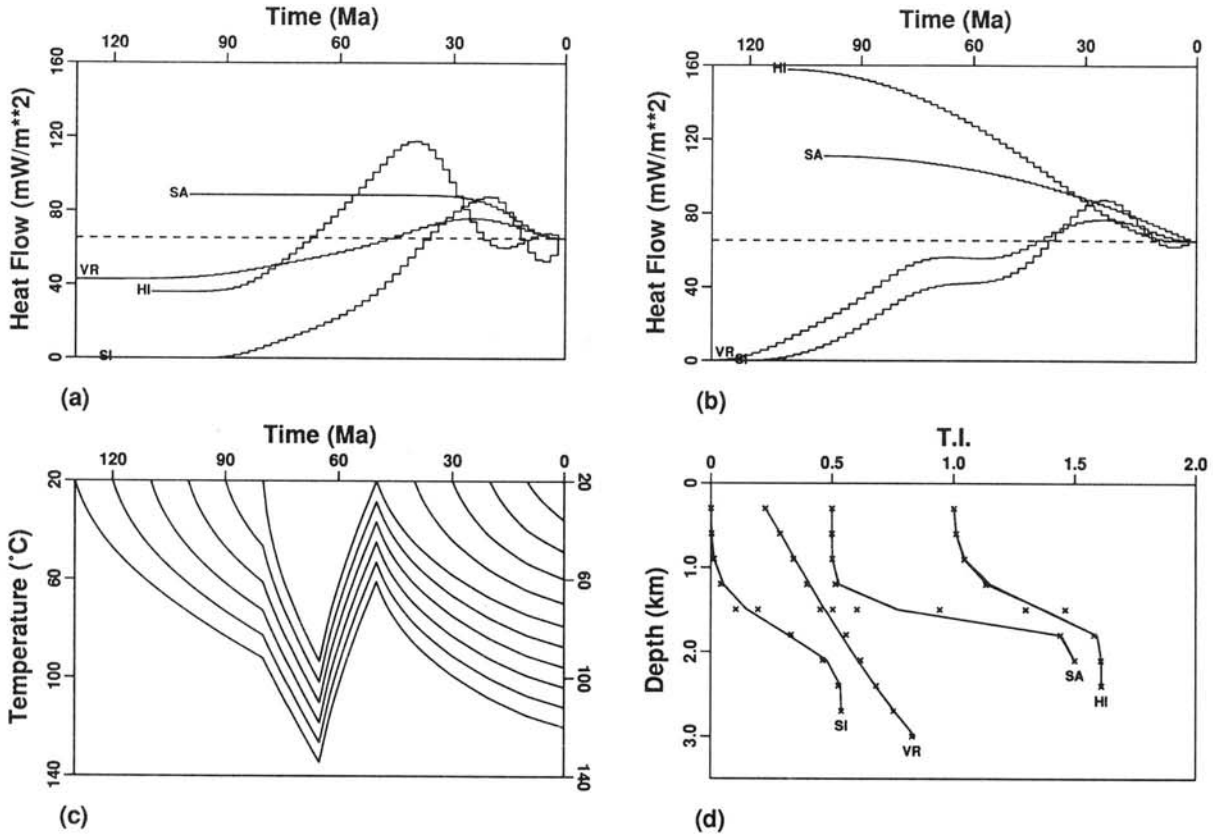

Figure 8. Results when the burial history includes an unconformity between 80 and 50 Ma in which 2 km of material was deposited, then eroded, as described in the text. The unconformity was modelled as a period of non-deposition for the inversion runs. The input data was calculated with $Q = 50\ \text{mW m}^{-2}$ and the present-day depth of the unconformity is 1.5 km. Other details as for Fig. 2.

various estimates have been published for the kinetic parameters used for the individual organic reactions. Here we examine the solutions obtained when the parameters in the maturation function used for the forward modelling step in the inversion procedure differ from those used to generate the synthetic data. For vitrinite reflectance we incorporate the maturation function proposed by Ritter (1984), which is similar to that of Royden *et al.* (1980), except $a = 1.35$ (see equation 5), which reduces the non-linear dependence on temperature. The Royden model predicts overall lower values than the Ritter model for a constant heat flow of $50\ \text{mW m}^{-2}$. In the inversion, we use the Royden model on data generated from the Ritter model and vice versa. The kinetic parameters used for the organic reactions are not particularly well constrained, partly as a result of the difficulty of extrapolating laboratory results to geological time-scales and because of the errors inherent in the observations, a range of kinetic parameters exist that will predict the data (Gallagher & Evans 1991). We only consider the role of inappropriate kinetic parameters for the two isomerization reactions and the values we use in the inversion are those suggested by Rullkötter & Marzi (1988). These are somewhat higher than those proposed by MacKenzie & McKenzie (1983), which were the values used in the forward model. The relevant values for these maturation functions are summarized in Table 2. The results of these inversion runs are given in Fig. 9 and it should be noted that none of the models reached their specific misfit

Table 2. Parameters used in the example with erroneous maturation functions (see Section 4.3.3). The vitrinite reflectance model is derived from Ritter (1984) and the kinetic parameters for the two organic reactions are from Rullkötter & Marzi (1988).

Model	function	parameter values
Vitrinite reflectance (Ritter model)	see eqs. 5,6	$a = 1.35$, $\alpha = 0.1$, $\beta = 0$
		$p = 0.16$, $q = -1.72$, Mt < 183.9
		$p = 0.30$, $q = -2.45$, 183.9 < Mt < 621.7
		$p = 0.49$, $q = -3.64$, Mt > 621.7
Sterane isomerisation (SI)	see eq. 14	$E_I = 169\ \text{kJmol}^{-1}$
		$A_I = 1.53 \times 10^{22}$/m.y.
Hopane isomerisation (HI)	see eq. 14	$E_I = 168\ \text{kJmol}^{-1}$
		$A_I = 2.55 \times 10^{22}$/m.y.

targets. The errors were specified as 0.004 units and to achieve convergence, the errors would have to be increased by an order of magnitude. The two vitrinite models behave as would be expected, VR1 (Ritter forward model, Royden inversion model) leads to an elevated heat flow to predict the deeper, but still under predicts the relatively high vitrinite reflectance values in the shallow section. VR2 (Royden forward model, Ritter inversion model) leads to a low overall heat flow history, but still over predicts the shallow data. The first and second derivative models give reasonably similar results which demonstrates that the data fitting dominates over the smoothness criterion. However, the heat flow histories obtained from the isomerization data

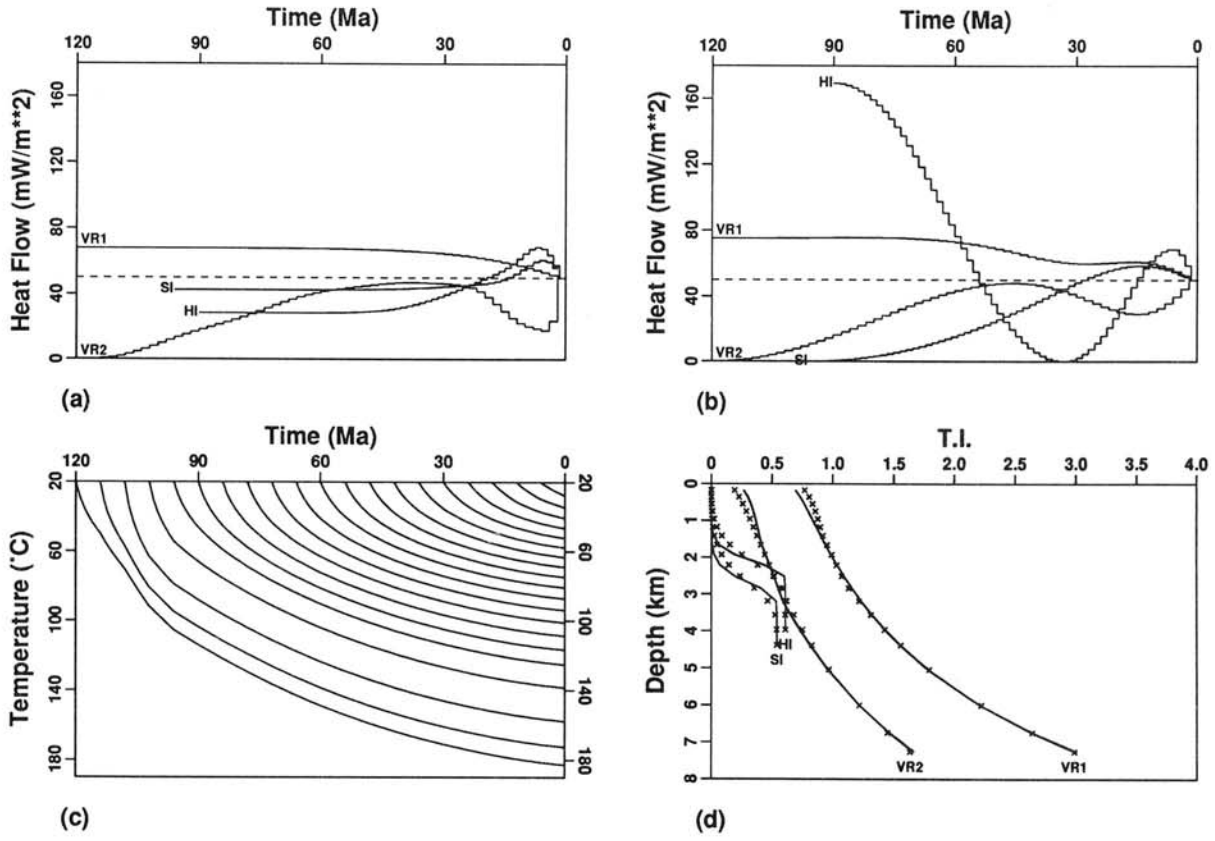

Figure 9. Results when incorrect maturation functions were used for the inversion. VR1 represents an inversion using the Royden model on data calculated with the Ritter model, and VR2 is the opposite. SI and HI represent the isomerization reactions where higher kinetic parameters were used in the inversion than for the forward model. The input data were calculated with $Q = 50\,\text{mW m}^{-2}$. Other details as for Fig. 2.

sets show more variation between the first and second derivative values, especially the hopane model. The models show consistent trends in over predicting the deeper data and under predicting the more shallow data, reflecting the increased reaction rate and higher critical temperature for higher kinetic parameters, as discussed in Section 4.2. The heat flow histories generally attempt to compensate for this by having relatively elevated heat flow in recent times and then decreasing below the true value of $50\,\text{mW m}^{-2}$ by about 30 Ma. The second derivative model for the hopane isomerization shows an extreme case of this compensation having a peak value of about $170\,\text{mW m}^{-2}$ at 90 Ma, a value of zero at about 30 Ma, while the most recent 10 Ma of the model agrees with the first derivative case.

5 CONCLUSION

The synthetic examples presented in this paper show that even with perfect data and the correct predictive model (including the burial history, thermal parameters and maturation functions), it will prove difficult to uniquely resolve variations of heat flow much beyond the time of maximum palaeotemperature. This conclusion could, to some extent, be deduced intuitively given the non-linear temperature dependence of the functions used to predict thermal indicators. Forward modelling may be used where the heat flow history is prescribed, thermal indicator levels predicted and compared to observations (e.g. MacKenzie & McKenzie 1983; Beaumont *et al.* 1985; Issler & Beaumont 1989; Deming & Chapman 1989; Burrus & Audebert 1990). While the forward models may predict the observed data adequately, we have demonstrated that there is an inherent non-uniqueness to such solutions. In other words, additional evidence would be required to constrain the appropriate geophysical model because the thermal indicator data would only be conclusive in disproving a particular model. We recommend that in seeking a single model (as nearly all authors tend to do) one should demand that the model be as simple as possible. In this work we have considered two types of simple model, i.e. those with minimal first and second derivatives. This approach has the advantage in that it does not depend on using a restrictive parametrization in order to achieve numerical stability and thereby avoids the implicit constraints that would be placed on the heat flow model. More importantly, it allows the user to gain insight into the degree of non-uniqueness of the problem and produces heat flow models which are free of unwarranted complexities which helps avoid the temptation for overinterpreting the data.

However, it is clear from the results of Section 4.2 that false structure can be introduced into the heat flow history. The apparent failure of our algorithm in these cases is due to the errors in the forward model, which are implicitly assumed to be negligible in this and nearly all inversion

studies. The complexity in the resulting models are not surprising and, in reality, if a variety of thermal indicators were available from a particular well, then such discrepancies between the individual heat flow different models would provide strong evidence that there is some inconsistency in the maturation functions. In this context, Lerche (1988a, b, 1990) has suggested that it is desirable to incorporate as many different thermal indicators as possible and find the heat flow that satisfies all data sets. Certainly any model should be able to adequately predict all data, but we would also recommend that inversion should be performed on individual data sets using an algorithm of the kind employed here as these can provide some insight into the reliability of a particular data set and its predictive function. Although we have considered seeking heat flow histories with minimal first and second derivatives, models with different properties may be sought. Any model property that can be written in the form of equation (24) can be handled by the algorithm (equation 25). An investigation of possible alternatives and their potential for retrieving information in the data may be a useful progression from this work.

ACKNOWLEDGMENTS

KG was supported during the initial part of this work through an Australian Government National Research Fellowship awarded to BHP, and subsequently by NERC.

REFERENCES

Abbot, G. D., Wang, G. Y., Eglinton, T. I., Home, A. K. & Petch, G. S., 1990. The kinetics of sterane biological marker release and degradation during the hydrous pyrolysis of vitrinite kerogen, *Geochim. Cosmochim. Acta,* **54,** 2451–2461.

Andrews-Speed, C. P., Oxburgh, E. R. & Cooper, B. A., 1984. Temperatures and depth dependent heat flow in the western North Sea, *Bull. Am. Assoc. Petrol. Geol.,* **68,** 1764–1781.

Angevine, C. L. & Turcotte, D. L., 1983. Oil generation in overthrust belts, *Bull. Am. Assoc. Petrol. Geol.,* **67,** 235–241.

Antia, D. D. J., 1986. Kinetic method for modelling vitrinite reflectance, *Geology,* **14,** 606–608.

Barker, C. E., 1983. Influence of time on metamorphism of sedimentary organic matter in liquid dominated geothermal systems, western North America, *Geology,* **11,** 384–388.

Barton, P. & Wood, R., 1984. Tectonic evolution of the North Sea basin: crustal stretching and subsidence, *Geophys. J. R. astr. Soc.,* **79,** 987–1022.

Beaumont, C., 1981. Foreland basins, *Geophys. J. R. astr. Soc.,* **65,** 291–329.

Beaumont, C., Boutilier, R., MacKenzie, A. S. & Rullkötter, J., 1985. Isomerisation and aromatisation of hydrocarbons and the paleothermometry and burial history of the Alberta foreland basin, *Bull. Am. Assoc. Petrol. Geol.,* **69,** 546–566.

Bethke, C. M., 1985. A numerical model of compaction driven groundwater flow and heat transfer and its application to the palaeohydrology of intracratonic sedimentary basins, *J. geophys. Res.,* **90,** 6817–6828.

Bond, G. C. & Kominz, M. A., 1984. Construction of tectonic subsidence curves for the lower Palaeozoic miogeocline, southern Canadian Rocky Mountains: implications for subsidence mechanisms, age of breakup and crustal thinning, *Geol. Soc. Am. Bull.,* **95,** 155–173.

Buck, W. R., Martinez, F., Steckler, M. S. & Cochran, J. R., 1988. Thermal consequences of extension: pure and simple, *Tectonics,* **7,** 213–234.

Burnham, A. K. & Sweeney, J. J., 1989. A chemical kinetic model of vitrinite maturation and reflectance, *Geochim. Cosmochim. Acta,* **53,** 2649–2658.

Burrus, J. & Audebert, F., 1990. Thermal and compaction processes in a young rifted basin containing evaporites: the Gulf of Lions, France, *Bull. Am. Assoc. Petrol. Geol.,* **74,** 1420–1440.

Castano, J. R., 1985. Uses of vitrinite reflectance in determining thermal history in sedimentary basins, *Bull. Am. Assoc. Petrol. Geol.,* **69,** 243.

Chapman, D. S., Keho, T. H., Bauer, M. S. & Picard, D. S., 1984. Heat flow in the Uinta Basin determined from bottom hole temperature (BHT) data, *Geophysics,* **49,** 453–466.

Cochran, J. R., 1983. Effects of finite rifting times on the development of sedimentary basins, *Earth planet. Sci. Lett.,* **66,** 289–302.

Constable, S., 1991. Comment on 'Magnetic appraisal using simulated annealing' by S. E. Dosso and D. W. Oldenburg, *Geophys. J. Int.,* **106,** 387–388.

Constable, S. C., Parker, R. L. & Constable, C. G., 1987. Occam's inversion: a practical algorithm for generating smooth models from electromagnetic sounding data, *Geophysics,* **52,** 289–300.

De Bredhoeft, J. D., Djevanshir, R. D. & Belitz, K., 1988. Lateral fluid flow in a compacting sand-shale sequence: South Caspian Basin, *Bull. Am. Assoc. Petrol. Geol.,* **72,** 416–424.

De Bremaecker, J. C., 1983. Temperature, subsidence and hydrocarbon maturation in extensional basins: a finite element model, *Bull. Am. Assoc. Petrol. Geol.,* **67,** 1410–1414.

Dembicki, H. Jr, 1984. An interlaboratory comparison of source rock data, *Geochim. Cosmochim. Acta,* **48,** 2641–2649.

Deming, D. & Chapman, D. S., 1989. Thermal histories and hydrocarbon generation: example from Utah–Wyoming Thrust Belt, *Bull. Am. Assoc. Petrol. Geol.,* **73,** 1455–1471.

Dow, W. G. & O'Connor, D. E., 1982. Kerogen maturity and type by reflected light microscopy applied to petroleum exploration, in *How to Assess Maturation and Palaeotemperatures,* pp. 133–157, ed. Staplin, F. L., Soc. Econ. Palaeontol. Mineral. short course no. 7.

Durand, B., ed., 1984. *Thermal Phenomena in Sedimentary Basins,* Collection Colloques et Seminaires 41, Editions Technip, Paris.

England, P. C., Oxburgh, E. R. & Richardson, S. W., 1980. Heat refraction and heat production in and around granite plutons in north-east England, *Geophys. J. R. astr Soc.,* **62,** 439–455.

Falvey, D. A., 1974. The development of continental margins in plate tectonic theory, *Aust. Petrol. Expl. Assoc. J.,* **14,** 95–106.

Fletcher, R., 1971. A modified Marquardt subroutine for non-linear squares, *Technical Report no. R6799,* AERE (UK) Harwell.

Gallagher, K., 1987. Thermal conductivity of sedimentary and basement rocks from the Eromanga and Cooper Basins, South Australia, *Expl. Geophys.,* **18,** 381–392.

Gallagher, K., 1988. The subsidence history and thermal state of the Eromanga and Cooper Basin, *PhD thesis,* Australian National University.

Gallagher, K. & Lambeck, K., 1989. Subsidence, sedimentation and sea-level changes in the Eromanga Basin, Australia, *Basin Res.,* **2,** 115–131.

Gallagher, K. & Evans, E., 1991. Estimating kinetic parameters for organic reactions from geological data: an example from the Gippsland Basin, Australia, *Appl. Geochem.,* **6,** in press.

Garg, S. K. & Kassoy, D. R., 1981. Convective heat and mass transfer in hydrothermal systems, in *Geothermal Systems: Principles and Case Histories,* pp. 37–76, eds Rybach, L. & Muffler, L. J. P., Wiley, New York.

Gleadow, A. J. W., Duddy, I. R. & Lovering, J. F., 1983. Fission track analysis: a new tool for the evaluation of thermal histories

and hydrocarbon potential, *Aust. Petrol. Expl. Assoc. J.*, **23,** 93–102.

Green, P. F., Duddy, I. R., Gleadow, A. J. W. & Lovering, J. F., 1989. Apatite fission track analysis as a palaeotemperature indicator for hydrocarbon exploration, in *Thermal Histories of Sedimentary Basins: Methods and Case Histories,* pp. 181–195. eds Naeser, N. D. & McCulloh, T. H., Springer-Verlag, Berlin.

Gretener, P. E. & Curtis, C. D., 1982. Role of temperature and time on organic metamorphism, *Bull. Am. Assoc. Petrol. Geol.*, **66,** 1124–1149.

Harrison, T. M. & Bé, K., 1983. $^{40}Ar/^{39}Ar$ spectrum analysis of detrital microclines from the southern San Joaquin Basin, California: an approach to determining the thermal evolution of sedimentary basins, *Earth planet. Sci. Lett.*, **64,** 244–256.

Hegarty, K. A., Weissel, J. K. & Mutter, J. C., 1988. Subsidence history of Australia's southern margin: constraints on basin, models, *Bull. Am. Assoc. Petrol. Geol.*, **72,** 615–633.

Hermanrud, C., Cao, S. & Lerche, I., 1990. Estimates of virgin rock temperature derived from BHT measurements: Bias and error, *Geophysics,* **55,** 924–931.

Hood, A., Gutjahr, C. C. & Heacock, R. L., 1975. Organic metamorphism and the generation of petroleum, *Bull. Am. Assoc. Petrol. Geol.*, **59,** 986–996.

Hutchinson, I., 1985. The effects of sedimentation and compaction on oceanic heat flow, *Geophys. J. R. astr. Soc.*, **82,** 439–459.

Issler, D. R., 1984. Calculation of organic maturation levels for offshore eastern Canada—implications for general application of Lopatin's method, *Can. J. Earth Sci.*, **21,** 477–488.

Issler, D. R. & Beaumont, C., 1989. A finite element model of the subsidence and thermal evolution of extensional basins: application to the Labrador continental margin, in *Thermal Histories of Sedimentary Basins: Methods and Case Histories,* pp. 239–267, eds Naeser, N. D. & McCulloh, T. H., Springer-Verlag, Berlin.

Jarvis, G. T. & McKenzie, D. P., 1980. Sedimentary basin formation with finite extension rates, *Earth planet. Sci. Lett.*, **48,** 42–52.

Jordan, T., 1981. Thrust loads and foreland basin evolution, Cretaceous, Western United States, *Bull. Am. Assoc. Petrol. Geol.*, **65,** 2506–2520.

Katz, B. J., Pheifer, R. N. & Schunk, D. J., 1988. Interpretation of discontinuous vitrinite reflectance profiles, *Bull. Am. Assoc. Petrol. Geol.*, **72,** 926–931.

Kominz, M. A. & Bond, G. C., 1986. Geophysical modelling of the thermal history of foreland basins, *Nature,* **320,** 252–256.

Lambeck, K., 1983. Structure and evolution of the intracratonic basins of central Australia, *Geophys. J. R. astr. Soc.*, **74,** 843–886.

Larter, S., 1989. Chemical models of vitrinite reflectance evolution, *Geol. Rundsch.*, **78,** 349–359.

Lerche, I., 1988a. Inversion of multiple thermal indicators: Quantitative methods of determining paleoheat flux and geological parameters I. Theoretical development for paleoheat flux, *Math. Geol.*, **20,** 1–36.

Lerche, I., 1988b. Inversion of multiple thermal indicators: Quantitative methods of determining paleoheat flux and geological parameters II. Development for chemical, physical and geological parameters, *Math. Geol.*, **20,** 73–96.

Lerche, I., 1990. *Quantitative Basin Analysis,* vol. 1. Academic Press, San Diego.

Lerche, I., Yarzab, R. F. & Kendall, C. G., 1984. Determination of palaeoheat flux from vitrinite reflectance data, *Bull. Am. Assoc. Petrol. Geol.*, **68,** 1704–1717.

Lopatin, N. V., 1971. Temperature and geologic time as factors in coalification, *Akad. Nauk. SSSR Izv. Ser. Geol.*, **3,** 95–106 (in Russian).

Lucazeau, F. & Le Douaran, S., 1985. The blanketing effect of basins formed by extension: a numerical model. Application to the Gulf of Lion and Viking Graben, *Earth planet. Sci. Lett.*, **74,** 92–102.

Mackenzie, A. S. & McKenzie, D. P., 1983. Isomerization and aromatization of hydrocarbons in sedimentary basins formed by extension, *Geol. Mag.*, **120,** 417–528.

Majorowicz, J. A., Jones, F. W., Lam, H. L. & Jessop, A. M., 1985. Terrestrial heat flow and geothermal gradients in relation to hydrodynamics in the Alberta Basin, Canada, *J. Geodyn.* **4,** 265–283.

Majorowicz, J. A., Jones, F. W., Ertman, M. E., Osadetz, K. G. & Stasiuk, L. D., 1990. Relationship between thermal maturation gradients geothermal gradients and estimates of the thickness of eroded foreland section, southern Alberta Plains, Canada, *Mar. Petrol. Geol.*, **7,** 138–152.

McKenzie, D. P., 1978. Some remarks on the development of sedimentary basins, *Earth planet. Sci. Lett.*, **40,** 25–32.

McKenzie, D. P., 1981. The variation of temperature with time and hydrocarbon maturation in sedimentary basins formed by extension, *Earth planet. Sci. Lett.*, **55,** 87–98.

Menke, W., 1984. *Geophysical Data Analysis: Discrete Inverse Theory,* Academic Press, San Diego.

Middleton, M. F., 1980. A model of intracratonic basin formation entailing deep crustal metamorphism, *Geophys. J. R. astr. Soc.*, **62,** 1–14.

Middleton, M. F., 1982. Tectonic history from vitrinite reflectance, *Geophys. J. R. astr. Soc.*, **68,** 121–132.

Naeser, N. D. & McCulloh, T. H., eds, 1989. *Thermal Histories of Sedimentary Basins: Methods and Case Histories,* Springer-Verlag, Berlin.

Peakman, T. M., ten Haven, H. L., Rechka, J. R., de Leeuw, J. W. & Maxwell, J. R., 1989. Occurrence of (20*R*)- and (20*S*)-$\Delta^{8(14)}$ and Δ^{14} 5α(H)-sterenes and the origin of 5α(H),14β(H),17β(H)-steranes in an immature sediment, *Geochim. Cosmochim. Acta,* **53,** 2001–2009.

Price, L. C., 1983. Geologic time as a parameter in organic metamorphism and vitrinite reflectance as an absolute palaeogeothermometer, *J. Petrol. Geol.*, **6,** 5–38.

Price, L. C., 1985. Geologic time as a parameter in organic metamorphism and vitrinite reflectance as an absolute palaeogeothermometer: reply, *J. Petrol. Geol.*, **8,** 233–240.

Price, L. C. & Barker, C. E., 1985. Suppression of vitrinite reflectance in amorphous rich kerogen. A major unrecognised problem, *J. Petrol. Geol.*, **8,** 59–84.

Ritter, U., 1984. The influence of time and temperature on vitrinite reflectance, *Org. Geochem.*, **6,** 473–480.

Royden, L. & Keen, C. E., 1980. Rifting process and thermal evolution of the continental margin of eastern Canada determined from subsidence curves, *Earth planet. Sci. Lett.*, **51,** 343–361.

Royden, L., Sclater, J. G. & Von Herzen, R. P., 1980. Continental margin subsidence and heat flow: Important parameters in formation of petroleum hydrocarbons, *Bull. Am. Assoc. Petrol. Geol.*, **64,** 173–187.

Rullkötter, J. & Marzi, R., 1988. Natural and artificial maturation of biological markers in a Toarcian shale from northern Germany, *Org. Geochem.*, **13,** 639–645.

Sajgó, Cs. & Lefler, J., 1986. A reaction kinetic approach to the temperature-time history of sedimentary basins, in *Paleogeothermics,* pp. 119–151, eds Buntebarth, G. & Stegana, L., Springer-Verlag, Berlin.

Sambridge, M. S., 1990. Non-linear arrival time inversion: constraining velocity anomalies by seeking smooth models in 3-D, *Geophys. J. Int.*, **102,** 653–677.

Shiboaka, M. & Bennett, A. J. R., 1977. Patterns of diagenesis in some Australian basins, *Aust. Petrol. Expl. Assoc. J.*, **17,** 58–64.

Sleep, N. H., 1971. Thermal effects of the formation of Altantic

continental margins by continental break-up, *Geophys. J. R. astr. Soc.*, **24,** 325–350.
Smith, L. & Chapman, D. S., 1983. On the thermal effects of groundwater flow 1. Regional scale systems, *J. geophys. Res.*, **88,** 593–608.
Stach, E., Mackowsky, M.-Th., Teichmüller, M., Taylor, G., Chandra, D. & Teichmüller, R., 1975. *Stach's Textbook of Coal Petrology*, Gerbrüder Borntraeger, Berlin.
Staplin, F. L., ed., 1982. *How to assess Maturation and Palaeotemperatures*, Soc. Econ. Palaeontol. Mineral. short course no. 7.
Steckler, J. S. & Watts, A. B., 1978. Subsidence of the Atlantic-type continental margin off New York, *Earth planet. Sci. Lett.*, **41,** 1–13.
Tarantola, A. & Valette, B., 1982. Inverse problems = Quest for information, *J. Geophys.*, **50,** 159–170.
Tilley, B. J., Nesbitt, B. E. & Longstaffe, F. J., 1989. Thermal history of Alberta deep basin: comparative study of fluid inclusion and vitrinite reflectance data, *Bull. Am. Assoc. Petrol. Geol.*, **73,** 1206–1222.
Tissot, B. P., Petet, R. & Ungerer, P., 1987. Thermal history of sedimentary basins, maturation indices, and hydrocarbon generation, *Bull. Am. Assoc. Petrol. Geol.*, **71,** 1445–1466.
Turcotte, D. L. & Angevine, C. L., 1982. Thermal mechanisms of basin formation, *Phil. Trans. R. Soc. Lond.*, A, **305,** 283–294.
Underwood, M. B., 1990. Temporal changes in geothermal gradient, Franscian subduction complex, northern California, *J. geophys. Res.*, **94,** 3111–3125.
Voorhoeve, H. & Houseman, G., 1987. The thermal evolution of lithosphere extending on a low angle detachment zone, *Basin Res.*, **1,** 1–10.
Waples, D., 1980. Time and temperature in petroleum formation: Application of Lopatin's method to petroleum exploration, *Bull. Am. Assoc. Petrol. Geol.*, **64,** 916–926.
Wernicke, B., 1985. Uniform sense normal simple shear of the continental lithosphere, *Can. J. Earth Sci.*, **22,** 108–125.
Wood, D. A., 1988. Relationships between thermal maturity indices calculated using Arrhenius equation and Lopatin method: Implications for petroleum exploration, *Bull. Am. Assoc. Petrol. Geol.*, **72,** 115–134.

APPENDIX

Partial derivatives of thermal indicators with respect to heat flow

When the heat flow is parametrized as block functions (equation 21a), the contribution to the maturation function for ith vitrinite reflectance value from the jth heat flow parameter is

$$Mt_i = \int_{t_{j-1}}^{t_j} a^{[\alpha(T_s+Q_j\kappa)-\beta]}\,dt' \tag{A1}$$

where

$$\kappa = \int_0^{z_i(t)} \frac{dz'}{K}$$

and $z_i(t)$ is the depth of the ith value at time t.

Similarly the contribution from the jth heat flow parameter to the ith value for the transformed aromatization and isomerization reactions may be written as

$$x_i' = \int_{t_{j-1}}^{t_j} \exp\left[-E_A/R(273.15 + T_s + Q_j\kappa)\right] dt', \tag{A2}$$

$$y_i' = \int_{t_{j-1}}^{t_j} \exp\left[-E_1/R(273.15 + T_s + Q_j\kappa)\right] dt', \tag{A3}$$

respectively, where T_s is the surface temperature in degrees Celsius. The partial derivatives of the thermal indicators x_i, y_i and Mt with respect to the jth heat flow parameter Q_j are

$$\frac{\partial Mt_i}{\partial Q_j} = \alpha \ln(a) \int_{t_{j-1}}^{t_j} \kappa a^{[\alpha(T_s+Q_j\kappa)-\beta]}\,dt', \tag{A4}$$

$$\frac{\partial x_i'}{\partial Q_j} = \frac{E_A}{R} \int_{t_{j-1}}^{t_j} \exp\left[-E_A/R(273.15 + T_s + Q_j\kappa)\right] \times \frac{\kappa}{(273.15 + T_s + Q_j\kappa)^2}\,dt' \tag{A5}$$

$$\frac{\partial y_i'}{\partial Q_j} = \frac{E_1}{R} \int_{t_{j-1}}^{t_j} \exp\left[-E_1/R(273.15 + T_s + Q_j\kappa)\right] \times \frac{\kappa}{(273.15 + T_s + Q_j\kappa)^2}\,dt'. \tag{A6}$$